1-1-2013

Magnetism and magnetic structures of PrMn2Ge2-xSix

Jianli Wang
University of Wollongong, jianli@uow.edu.au

S J. Campbell
University of New South Wales, stewart.campbell@adfa.edu.au

M Hofmann
Technical University of Munchen

S J. Kennedy
ANSTO

R Zeng
University of Wollongong, rzeng@uow.edu.au

See next page for additional authors

Magnetism and magnetic structures of PrMn2Ge2-xSix

Abstract

The structural and magnetic properties of seven PrMn2Ge2-xSix compounds with Si concentrations in the range x = 0.0-2.0 have been investigated by x-ray diffraction, magnetic (5- 350 K), differential scanning calorimetry (300-500 K) and neutron diffraction (3-480 K) measurements. Replacement of Ge by Si leads to a contraction of the unit cell and significant modifications to the magnetic states-a crossover from ferromagnetism at room temperature for Ge-rich compounds to antiferromagnetism for Si-rich compounds. The compositional dependence of the room temperature lattice parameters exhibits non-linear behaviour around x = 1.2, reflecting the presence of magnetovolume effects. Re-entrant ferromagnetism has been observed in both PrMn2Ge1.0Si1.0 and PrMn2Ge0.8Si1.2 compounds with co-existence of canted ferromagnetism and canted antiferromagnetism detected, with both compounds exhibiting a larger unit cell volume in the canted Fmc state than in the canted AFmc.Combined with earlier studies of this system, the magnetic phase diagram has been constructed over the full range of PrMn2Ge2-xSix compositions (x = 0.0-2.0) and over the temperature range of interest (T = 3- 480 K). In common with other systems in the RMn2X2 series, the overall magnetic behaviour of PrMn2Ge2-xSix compounds is governed by the strong dependence of the magnetic couplings on the Mn-Mn spacing within the ab-plane. Both total manganese moment [Formula: see text] and in-plane manganese moment [Formula: see text] at 5 K are found to decrease with increasing Si content, which can be ascribed to the reduction of Mn-Mn separation distance and stronger Si- Mn hybridization compared with Ge-Mn hybridization. Pr site ferromagnetic ordering occurs for x < 1.6 below

Keywords

magnetism, structures, magnetic, prmn2ge2, xsix

Disciplines

Engineering | Physical Sciences and Mathematics

Publication Details

Wang, J. L., Campbell, S. J., Hofmann, M., Kennedy, S. J., Zeng, R., Md Din, M. F., Dou, S. X., Arulraj, A. & Stusser, N. (2013). Magnetism and magnetic structures of PrMn2Ge2-xSix. Journal of Physics: Condensed Matter, 25 (38), 386003-1-386003-13.

Authors

Jianli Wang, S J. Campbell, M Hofmann, S J. Kennedy, R Zeng, M Md Din, S X. Dou, A Arulraj, and N Stusser

Magnetism and Magnetic Structures of $PrMn_2Ge_{2-x}Si_x$

J. L. Wang[a,b,c], S. J. Campbell[c], M. Hofmann[d], S. J. Kennedy[a], R. Zeng[b], M.F. Md Din[b], S. X. Dou[b], A. Arulraj[e] and N. Stusser[e]

[a]Bragg Institute, ANSTO, Lucas Heights, NSW 2234 Australia

[b]Institute for Superconductivity and Electronic Materials, University of Wollongong, Wollongong, NSW 2522 Australia

[c]School of Physical, Environmental and Mathematical Sciences, The University of New South Wales Canberra at The Australian Defence Force Academy, ACT 2600, Australia

[d]FRM-II, Technische Universität München, 85747 Garching, Germany

[e]BER II, Lise Meitner Campus, HZB, Hahn-Meitner-Platz-1, D-14109 Berlin, Germany

Abstract: The structural and magnetic properties of seven $PrMn_2Ge_{2-x}Si_x$ compounds with Si concentrations in the range x=0.0 - 2.0 have been investigated by X-ray diffraction, magnetic (5-350 K), differential scanning calorimetry (300-500 K) and neutron diffraction (3-480 K) measurements. Replacement of Ge by Si leads to a contraction of the unit cell and significant modifications to the magnetic states - a crossover from ferromagnetism at room temperature for Ge-rich compounds to antiferromagnetism for Si-rich compounds. The compositional dependence of the room temperature lattice parameters exhibits non-linear behaviour around x=1.2 reflecting the presence of magnetovolume effects. Re-entrant ferromagnetism has been observed in both $PrMn_2Ge_{1.0}Si_{1.0}$ and $PrMn_2Ge_{0.8}Si_{1.2}$ compounds with co-existence of canted ferromagnetism and canted antiferromagnetism detected with both compounds exhibiting a larger unit cell volume in the canted F*mc* state than in the canted AF*mc*.

Combined with earlier studies of this system, the magnetic phase diagram has been constructed over the full range of $PrMn_2Ge_{2-x}Si_x$ compositions (x=0.0-2.0) and over the temperature range of interest (T=3-480 K). In common with other systems in the RMn_2X_2 series, the overall magnetic behaviour of $PrMn_2Ge_{2-x}Si_x$ compounds is governed by the strong dependence of the

magnetic couplings on the Mn-Mn spacing within the *ab*-plane. Both total manganese moment μ_{tot}^{Mn} and in-plane manganese moment μ_{ab}^{Mn} at 5 K are found to decrease with increasing Si content which can be ascribed to the reduction of Mn-Mn separation distance and stronger Si-Mn hybridization compared with Ge-Mn hybridization. Pr site ferromagnetic ordering occurs for $x < 1.6$ below T_C^{Pr}.

Key words: magnetic phase transition, phase diagrams, neutron diffraction, rare earth metals and alloys

PACS: 75.30.Kz; 74.62.-c, 61.05.F-, 71.20.Eh

1. Introduction

The rare earth compounds RMn_2X_2 with X=Si or Ge crystallise in the body centred tetragonal $ThCr_2Si_2$-type structure with space group *I*4/*mmm*. The R, Mn and X atoms occupy the 2a, 4d and 4e sites respectively with the different atoms stacked along the c-axis in the layered sequence ... R–X–Mn–X–R .... The RMn_2X_2 series of compounds have continued to attract a great deal of attention over the past two decades due to their natural layered crystal structure and interesting range of physical properties and phenomena such as coupled magnetic and crystallographic transitions or valence-related transitions, superconductivity, heavy fermion and Kondo behaviour [1, 2 and references therein]. Due to the fact that the magnetic states of Mn-sublattice depend sensitively on the inter-planar and intra-planar Mn-Mn distances, RMn_2X_2 alloys have been found to exhibit a vast variety of magnetic structures and magnetic phase transitions with change in external factors such as temperature, pressure and field and, as a result, making them model systems for the study of the volume dependence of magnetic ordering in intermetallic compounds [e.g. 3, 4]. This type of system therefore offers scope for design of critical magnetic parameters – such as the type or order of magnetic phase transitions and ability to shift transition temperatures - by controlling the intra-planar separation distance $d^a_{Mn\text{-}Mn}$ with applied [4, 5] or chemical pressure [2, 6] (via substitution with elements of different atomic sizes).

The notations used to describe the magnetic structure type and critical transition temperatures in this paper are defined in refs [7-10]. $PrMn_2Ge_2$ exhibits four magnetic transitions below 500 K [7, 10]). On decreasing temperature, it exhibits five magnetic states: (1) paramagnetism (PM), (2) intralayer antiferromagnetic within ab-plane (AF*l*), (3) ferromagnetic mixed commensurate structure (F*mc),* (4) ferromagnetic mixed incommensurate structure (F*mi*) and (5) ferromagnetic mixed incommensurate structure plus Pr moments coupled ferromagnetically along the *c*-axis parallel to the Mn moments (F*mi* + F(*Pr*)). With decreasing temperature from PM region, T_N^{intra} (=415 K) defines the magnetic transition from PM to AF*l*; T_C^{inter} (=330 K) defines the transition

from AF*l* to F*mc*; $T_{c/c}$ (=280 K) defines the transformation of magnetic structure from F*mc* to F*mi* and T_C^{Pr} (80 K) defines the transition temperature for onset of the ordering of the Pr sublattice [10].

$PrMn_2Si_2$ is relatively simple with a collinear antiferromagnetic structure (AF*il*) below T_N^{inter} (= 368 K) reported from neutron diffraction measurements [8]. A more recent study indicates that there should be two magnetic phase transitions rather than only one when the samples is cooled from the paramagnetic state: first a transition from PM to AF*l* at T_N^{intra} (=450 K) followed by a transition from AF*l* to AF*mc* at T_N^{inter} (=355 K) [9]. A crossover from the ferromagnetic ordering of $PrMn_2Ge_2$ at room temperature (lattice constant a = 4.123 Å) to the room temperature antiferromagnetic ordering of $PrMn_2Si_2$ (a = 4.026 Å) is therefore expected to take place on replacing Ge with Si in $PrMn_2Ge_2$ due to the difference in atomic sizes between Si (atomic radius r = 1.32 Å) and Ge (r = 1.37 Å) [10, 11]. The structural and magnetic properties of $PrMn_2Ge_{2-x}Si_x$ compounds have been investigated over the composition range x=0 - 2 by X-ray powder diffraction, AC susceptibility and differential scanning calorimetry [10]. This has led to a discovery of crossover from ferromagnetic ordering for $PrMn_2Ge_2$ to antiferromagnetic ordering for $PrMn_2Si_2$ as a function of Si concentration x although accurate magnetic structures have yet to be determined for x = 0.4 - 1.6. As well the type of some magnetic phase transitions, such as the spin reorientation around T_{sr}=118 K for x=1.6, remain to be clarified fully [10].

Interest in the behaviour of layer structure materials has been enhanced in recent years by the discovery of a giant magnetocaloric effect (MCE) near room temperature in $Gd_5Si_2Ge_2$ [see 12 and reference therein]. $R_5(Si,Ge)_4$ type compounds have a distinct layered structure in which the covalent Si-Si, Si-Ge, and Ge-Ge bonds and interlayer distances play a vital role in determining their magnetic and magnetocaloric properties [12]; attention has therefore increasingly focussed on understanding the fundamental properties of this type of layered material. As already noted the $PrMn_2Ge_{2-x}Si_x$ system has a sequence of atomic layers stacked along the c-axis similar to the $R_5(Si,Ge)_4$ system. The relatively simple body centred tetragonal $ThCr_2Si_2$-type structure offers scope for selection of the magnetic state via control of the intra-planar separation distance $d^a_{Mn\text{-}Mn}$,

thus allowing a template for enhanced understanding of the correlation between magnetic properties and atomic distances. In this paper we present the results of an investigation of the crystallographic and magnetic properties of $PrMn_2Ge_{2-x}Si_x$ compounds with x=0.0 - 2.0 by x-ray diffraction, magnetic, differential scanning calorimetry and neutron diffraction measurements. This has enabled us to establish the magnetic structures of the different magnetic states and complete the magnetic phase diagram of $PrMn_2Ge_{2-x}Si_x$.

2. Experimental

$PrMn_2Ge_{2-x}Si_x$ alloys with Si concentrations x=0.0, 0.4, 0.8, 1.0, 1.2, 1.6 and 2.0 were prepared by arc melting the high purity elements on a water-cooled Cu hearth under purified argon gas. The mass loss of Mn during melting has been compensated for by adding 3% excess Mn. The ingots were melted five times to attain homogeneity and then annealed at 900°C for one week in an evacuated quartz tube. The samples were characterized by x-ray diffraction (CuK_α; λ = 1.5418 Å). The temperature dependence of the magnetization, *M(T)*, was measured in a magnetic field of B_{appl} = 0.01 T in a superconducting quantum interference device (SQUID) from 5 K to 350 K. All samples were investigated by differential scanning calorimetry (DSC) to check for possible phase transitions in the higher temperature range from 300 K to 500 K. Neutron diffraction patterns were collected on diffractometer E6, BENSC, Berlin (λ = 2.44 Å) over the temperature range 3-480 K to cover the temperature range over which long range magnetic order was observed. Further details were obtained on the Wombat (high intensity; λ = 2.4072 Å) and Echidna (high resolution; λ = 1.622 Å) diffractometers, OPAL, Australia.

3. Results

3.1 X-ray Diffraction – Structural Behaviour

Rietveld refinements [Fullprof package; 13] of the room temperature x-ray diffraction patterns indicate that all of the $PrMn_2Ge_{2-x}Si_x$ samples crystallize in the $ThCr_2Si_2$ structure and that any

impurity is less than 2% for Si rich samples (Pr_2O_3; Pr_5Si_4). The refined results - including lattice parameters *a*, *c*, axial ratio *c*/*a* and unit cell volume V - are shown in Fig. 1. As expected substitution of Ge by Si leads to a monotonic decrease of both *a* and *c* along with concomitant contraction of the unit cell volumes with increasing Si content (e.g. dV/dx ~ -7.34 $Å^3$ [11]) with good agreement being obtained with published results [10]. However, it is noted that the variation of the lattice constants and unit cell volume change slope with composition around x=1.0-1.2 (Figs 1(a), (c)) with this behaviour evident in the composition dependence of the ratio *c/a* (Fig. 1(b). This change in slope around x=1.0-1.2 is likely to be related to the change in magnetic ordering of the Mn-sublattice as presented in Section 3.3. At room temperature compounds with x ≤ 1.2 are in a ferromagnetic state (or mixed ferromagnetic + antiferromagnetic state) while the compounds with x > 1.2 are purely antiferromagnetic [10]. Similar tendencies in the composition dependence of the lattice constants have been detected in the related $PrMn_{2-x}Fe_xGe_2$ system [14].

As is well known RMn_2X_2 (X=Ge or Si) compounds exhibit different magnetic behaviours around two critical values of the lattice parameter *a* - a_{crit1}=4.02 Å and a_{crit2}=4.06 Å [1, 2] - with RMn_2X_2 compounds displaying the following general behaviour.

- Ferromagnetic interlayer alignment and antiferromagnetic intralayer (within the *a*-*b* plane*)* alignment (F*mc* or F*mi*) for $a > a_{crit2}$=4.06 Å.
- Antiferromagnetic intralayer and interlayer alignment (AF*mc* or AF*mi*) for a_{crit2}=4.06 Å > *a* > a_{crit1}=4.02 Å.
- The absence of an in-plane spin component and antiferromagnetic interlayer coupling (AF*il* type) for $a < a_{crit1}$=4.02 Å [1, 2].

As shown in Fig. 1, for $PrMn_2Ge_{2-x}Si_x$ samples of Si composition x <~ 1.4, the room temperature lattice constant *a* is larger than the first critical value a_{crit2}. As confirmed in Section 3.3, crossing this structural threshold indicates that a crossover from ferromagnetic ordering to antiferromagnetic ordering $PrMn_2Ge_{2-x}Si_x$ is expected to take place around x~1.4 (see also Table 2).

3.2 Magnetic Measurements

In discussing the magnetic regions for the seven $PrMn_2Ge_{2-x}Si_x$ samples (x=0.0 – 2.0), the transition temperatures are identified with their predominant physical influence. The magnetic behaviours of the seven $PrMn_2Ge_{2-x}Si_x$ samples are considered below with increase in Si concentration.

1. $PrMn_2Ge_2$, $PrMn_2Ge_{1.6}Si_{0.4}$, $PrMn_2Ge_{1.2}Si_{0.8}$

The magnetization and DSC curves for $PrMn_2Ge_2$, $PrMn_2Ge_{1.6}Si_{0.4}$ and $PrMn_2Ge_{1.2}Si_{0.8}$ are found to exhibit similar features. As an example, Figure 2 shows the composite magnetization and DSC data over the temperature range ~5 - 500 K for $PrMn_2Ge_{1.6}Si_{0.4}$. The $PrMn_2Ge_{1.6}Si_{0.4}$ compound behaves in a similar way to $PrMn_2Ge_2$ [7] with four magnetic phase transitions observed between 5–500 K as marked by the arrows. The transitions are indicated as T_C^{Pr}, $T_{c/c}$, T_C^{inter} and T_N^{intra} with increasing temperature, respectively.

Below 340 K for the $PrMn_2Ge_{1.6}Si_{0.4}$ sample, two magnetic phase transitions are readily detected at T_C^{Pr} ~51 K and T_C^{inter} ~ 325 K with a third phase transition likely around $T_{c/c}$ ~167 K as indicated by the change in slope of the *M* versus *T* curve noted in Fig. 2. We have determined T_C^{Pr} and $T_{c/c}$ from the derivative of the magnetization data with respect to temperature with the transition at $T_{c/c}$ ~167 K shown to be more evident in the d*M*/d*T* curve as in the insert of Fig. 2. The magnetic response around T_C^{inter} ~325 K indicates a ferromagnetic macroscopic behaviour which can be ascribed to the transformation from a higher temperature antiferromagnetic state to a lower temperature ferromagnetic state [7]. Similarly, in comparison with the behaviour of $PrMn_2Ge_2$ [7], the transition at T_C ~51 K for $PrMn_2Ge_{1.6}Si_{0.4}$ can be attributed to T_C^{Pr} where the Pr-sublattice becomes magnetically ordered [7]. From the DSC measurements, two transitions are detected around T_C^{inter} ~325 K and T_N^{intra} ~428 K with the transition around T_C^{inter} ~325 K agreeing well with the observations from the region of overlap with the magnetization measurements. As in Section 3.3, the transition T_N^{intra} ~428 K is shown to represent the phase transition from paramagnetism to the antiferromagnetic state (T_N^{intra}).

2. $PrMn_2Ge_{1.0}Si_{1.0}$ and $PrMn_2Ge_{0.8}Si_{1.2}$

Both $PrMn_2Ge_{1.0}Si_{1.0}$ and $PrMn_2Ge_{0.8}Si_{1.2}$ compounds reveal similar re-entrant ferromagnetic behaviour with four magnetic phase transitions below 500 K. The composite magnetization versus temperature and DSC curve is shown in Figure 3(a) for $PrMn_2Ge_{1.0}Si_{1.0}$. The sharp increase of magnetization below T_C^{inter}~311 K reflects ferromagnetic character below this transition temperature while the decrease in magnetization below T_N^{inter}~200 K signals the presence of an antiferromagnetic component at lower temperatures. The magnetization increases again below T_C^{Pr}~66 K consistent with magnetic ordering of the Pr-sublattice. For temperatures up to 500 K, the DSC experiments indicate the fourth phase transition T_N^{intra}~425 K which can be ascribed to the transformation from high temperature PM to a lower temperature AF*l*.

For $PrMn_2Ge_{0.8}Si_{1.2}$, the four transition temperatures equivalent to those observed in $PrMn_2Ge_{1.0}Si_{1.0}$ are derived to be T_N^{intra}~435 K, T_C^{inter}~303 K, T_N^{inter}~178 K and T_C^{Pr}~54 K. However, in comparison with the behaviour of several other re-entrant ferromagnetic systems such as $PrMn_{1.4}Fe_{0.6}Ge_2$ [6] and $SmMn_2Ge_2$ [15], the magnetization for both compounds $PrMn_2Ge_{1.0}Si_{1.0}$ and $PrMn_2Ge_{0.8}Si_{1.2}$ in the antiferromagnetic region between T_C^{Pr} and T_N^{inter} does not attain zero (see Figs. 3(a) and (b)). This behaviour indicates that formation of the antiferromagnetic state is incomplete and there exists the possibility for co-existence of antiferromagnetism and ferromagnetism. In fact the co-existence of ferromagnetic and antiferromagnetic states has been found in other RMn_2X_2 systems as first reported for $La_{0.8}Y_{0.2}Mn_2Si_2$ [16]. The co-existence of antiferromagnetism and ferromagnetism in $PrMn_2Ge_{1.0}Si_{1.0}$ and $PrMn_2Ge_{0.8}Si_{1.2}$ has been confirmed by our neutron diffraction results (Section 3.3).

It is clear from the three dimensional thermomagnetic curves for $PrMn_2Ge_{0.8}Si_{1.2}$ (magnetisation; field, temperature; Fig. 3(b)) that the width of both the lower and higher temperature F*mc* phase regions extend with applied magnetic field, while the AF*mc* range correspondingly becomes narrower. These field induced changes (indicated by the lengths of the arrows along the temperature axis in Fig. 3(b)) demonstrate that the applied magnetic field destroys

the AF*mc* state in $PrMn_2Ge_{0.8}Si_{1.2}$. This observation has been confirmed by the appearance of field-induced metamagnetic phase transitions [11] in the magnetization curves of $PrMn_2Ge_{0.8}Si_{1.2}$ as shown in Fig. 4(a) (while we have measured the field dependence of magnetization at different magnetic states from 10 K to 340 K in 5 K steps, for clarity only the M-B curves at 10 K, 120 K, 250 K and 340 K are re-plotted as typical examples in Fig. 4(a)). The corresponding Arrot plots [17] of M^2 against B/M at 10 K, 120 K, 250 K and 340 K are shown in Fig. 4(b). The positive intercepts on the M^2 axis at 10 K and 250 K demonstrates clearly that $PrMn_2Ge_{0.8}Si_{1.2}$ is ferromagnetic at these temperatures while the negative intercept on the M^2 axis at 120 K and 340 K demonstrates that $PrMn_2Ge_{0.8}Si_{1.2}$ is antiferromagnetic at these temperatures [11, 14, 17]. In addition, a distinct jump in magnetization has been found at B~2 T for the M-B curve at 120 K where $PrMn_2Ge_{0.8}Si_{1.2}$ is antiferromagnetic at low fields B < 2 T. This feature (marked by an arrow in Fig. 4(a)) indicates a field-induced metamagnetic phase transition from an antiferromagnetic to a ferromagnetic state at B~2 T (similar behaviour has been detected in $PrMn_{1.4}Fe_{0.6}Ge_2$ [6]). This metamagnetic transition at B_{cr}~2 T is more evident from the d*M*/d*B* versus *B* curve shown as the inset to Fig. 4(b). Fig. 4(c)) shows the variation of the critical fields B_{cr} for the metamagnetic AF to FM transition as obtained from graphs of *dM/dB* versus *B* across the temperature region 55 K to 160 K. Similar to the behaviour found in $SmMn_2Ge_2$ [4], the temperature dependence of the critical fields B_{cr} in the regions around T_C^{Pr} and T_N^{inter} (Fig. 4(c)) shows clearly that the closer to the transition temperature (in this case T_C^{Pr} and T_N^{inter}), the smaller the magnetic field that is needed to induce the metamagnetic transition from antiferromagnetism to ferromagnetism. For example, at 65 K, a temperature close to the transition T_C^{Pr}~54 K a field of B_{cr}~1.1 T is required, and similarly at 160 K close to the transition T_N^{inter}~178 K a field of B_{cr}~1.1 T is required to induce the metamagnetic transition. By comparison at 100 K, relatively far removed from either transition temperature, a field of ~2.4 T is required to induce the metamagnetic transition. Figs 3(b) and 4(c) demonstrate clearly that an applied magnetic field stabilizes the ferromagnetic state as expected rather than the antiferromagnetism state [6, 14].

The Arrott plot method [17] is useful as a direct tool for distinguishing first order magnetic transitions from second order magnetic transitions [11, 14]. The nature of the transition - second-order or first-order - is indicated by a positive or negative slope in the isothermal plots of M^2 versus B/M respectively. In the case of $PrMn_2Ge_{0.8}Si_{1.2}$, the negative slope of the Arrott plot at 120 K in Fig. 4(b) indicates the first-order nature of this metamagnetic phase transition from an AF state to a FM state. This agrees well with the appearance of the temperature hysteresis of about 6 K observed in the temperature dependence of magnetization between the cooling (C) and warming (W) processes [11].

3. $PrMn_2Ge_{0.4}Si_{1.6}$, $PrMn_2Si_2$

As indicated by the magnetisation and DSC measurements of Figures 5(a) and 5(b), both $PrMn_2Ge_{0.4}Si_{1.6}$ and $PrMn_2Si_2$ exhibit two magnetic phase transitions above room temperature. The transitions are assigned as T_N^{inter}~335 K and T_N^{intra}~371 K for $PrMn_2Ge_{0.4}Si_{1.6}$ and T_N^{inter}~328 K and T_N^{intra}~355 K for $PrMn_2Si_2$. In addition further anomalies are evident at ~282 K for $PrMn_2Ge_{0.4}Si_{1.6}$ and ~ 159 K for $PrMn_2Si_2$. As considered in analysis of the neutron diffraction results (section 3. 3), in the case of $PrMn_2Ge_{0.4}Si_{1.6}$ the anomaly may indicate a spin reorientation of the Mn moments at T_{sr}~282 K or the presence of weak ferromagnetism. Given the increase in magnetisation around ~282 K and the sharp increase in magnetization below ~50 K, we have measured the field dependences of the magnetization at 5 K, 50 K, 100 K and 260 K in order to test for possible ferromagnetic character below ~282 K. Both the M-B curves and the corresponding Arrot plots indicated that $PrMn_2Ge_{0.4}Si_{1.6}$ remains antiferromagnetic above and below ~50 K the temperature at which the anomaly of magnetization occurs in the M versus T curve of Fig. 5(a). Similar behaviour has been found for $PrMn_{1.2}Fe_{0.8}Ge_2$ [6] where a sudden increase in the magnetization is also detected below 20 K (T_N^{inter} ~ 154 K) but with no evidence of a magnetic phase transition around 20 K. By comparison for $PrMn_2Si_2$, Dincer *et al.* [9] reported transition temperatures T_N^{inter} =355 K and T_N^{intra} =450 K based on their susceptibility measurements (up to 600 K) and neutron study to 300 K. In addition they detected an anomaly around 240 K which they

ascribed to T_C^{intra} - reflecting the presence of weak ferromagnetic components of the ordered Mn moments [9]. It is worth noting that the anomaly around 240 K [9] is similar to the anomaly identified around 159 K in the present $PrMn_2Si_2$ sample (Fig. 5(b)).

3.3 Neutron Diffraction

A set of neutron powder diffraction patterns was obtained for four selected $PrMn_2Ge_{2-x}Si_x$ samples (x=0.4, 1.0, 1.2, 1.6) over the temperature range 3 - 480 K. Rietveld refinements were carried out on all patterns using the FULLPROF program package [13] which allows us to derive the structural and magnetic parameters. As explained fully in related articles [2, 6, 9, 18, 20], the specific location of Mn atoms on the 4d site in the $ThCr_2Si_2$ structure (space group *I4/mmm*) allows ready identification of various magnetic structures from key indicators in the neutron diffraction patterns as follows.

(1) Ferromagnetic ordering of the Mn atoms – hkl reflections with h + k = 2n and l = 2n; (e.g. (112), (200) reflections);

(2) Antiferromagnetic ordering of the Mn atoms within the (001) planes - reflections with h +k = 2n +1; (e.g. (101), (103) reflections);

(3) Collinear antiferromagnetic structure between adjacent Mn planes - reflections with h + k + l = 2n + 1; (e.g. (111), (113) reflections;

(4) Ferromagnetic mixed incommensurate structure (Fmi) of wavevector (0, 0, q_z) - satellite reflections with h + k = 2n + 1; (e.g. (101), (103)).

1. $PrMn_2Ge_{1.6}Si_{0.4}$

As shown in Fig. 6, neutron diffraction patterns were obtained for $PrMn_2Ge_{1.6}Si_{0.4}$ at selected temperatures to cover the magnetic regions between the magnetic transitions indicated in Fig. 2. Refinement of the 480 K neutron diffraction pattern confirms that $PrMn_2Ge_{1.6}Si_{0.4}$ is paramagnetic at this temperature. At 340 K (i.e. below T_N^{intra} ~ 428 K; Fig. 2) the intensity of the (101) reflection increases, and consistent with neutron diffraction condition (2) above, $PrMn_2Ge_{1.6}Si_{0.4}$ exhibits the

AF*l* structure. At 292 K, below transition temperature T_C^{inter}~325 K, the appearance of the (112) peak together with the magnetic intensity at (101) characterizes the formation of the F*mc* structure (satisfying both neutron diffraction conditions (1) and (2)). The canting angle has been determined to be 62.2° with respect to the *c*-axis at 292 K. Similarly, at 150 K (i.e. below $T_{c/c}$~167 K), the presence of satellites peaks $(101)^+$, $(101)^-$ and $(103)^+$, $(103)^-$ in the patterns together with diffraction condition (4) above, clarifies that the magnetic feature observed at ~167 K in the M versus T and dM/dT versus T curves of Fig. 2, reflects a magnetic phase transition from F*mc* for $T>T_{c/c}$~167 K, to F*mi* for $T<T_{c/c}$~167 K. Finally, the increase in the magnetization below T_C^{Pr}~51 K together with the intensity of both the (101) and (112) reflections at 5 K compared with their intensities at 150 K as in the diffraction patterns of Fig. 6, indicates that the Pr moments of the Pr sublattice align parallel with Mn–moments along the c-axis [8, 14]. At 5 K, the values of the magnetic moments are derived to be μ_c^{Mn}= 2.24 μ_B, μ_{ab}^{Mn}= 2.23 μ_B and μ_c^{Pr}= 1.52 μ_B with the magnitude of the propagation vectors q_z= 0.226±0.002. By comparison, the values of q_z for $PrMn_2Ge_2$ and $PrMn_2Ge_{1.2}Si_{0.8}$ at 7 K also have been derived to be q_z= 0.274±0.002 and q_z= 0.166±0.003, respectively. So, it can be concluded that the replacement of Si for Ge leads to a decrease in q_z. Similar behaviour has been detected for the replacement of Fe for Mn [14] and Y [18] or Lu [2] for Pr in $PrMn_2Ge_2$ compound where a reduction of q_z has been detected. The temperature dependences of the structural and magnetic parameters of $PrMn_2Ge_{1.6}Si_{0.4}$ as derived from the refinements are shown in Figs. 7(a), (b) and (c). Even though the number of data points is relatively sparse, Fig. 7(b) reveals a significant change in the temperature dependence of the *c/a* ratio around T_C^{inter}; this indicates that strong coupling occurs between magnetism and crystal lattice in the presence of a c-axis component of Mn moment. Theses effects are also observed in the $PrMn_{2-x}Fe_xGe_2$ system [14] where the presence of the interlayer Mn–Mn interactions rather than the intralayer Mn–Mn interactions play the major role in the anomalous thermal expansion observed at magnetic transition in these layered systems, with the interlayer Mn–Mn interactions governing the significant magnetovolume effects.

2. $PrMn_2Ge_{1.0}Si_{1.0}$ and $PrMn_2Ge_{0.8}Si_{1.2}$

Given the complicated re-entrant ferromagnetic behaviour exhibited by $PrMn_2Ge_{1.0}Si_{1.0}$ and $PrMn_2Ge_{0.8}Si_{1.2}$ compared with $PrMn_2Ge_{1.6}Si_{0.4}$, neutron diffraction patterns were collected using temperature steps of around 25 K for $PrMn_2Ge_{1.0}Si_{1.0}$ and 20 K for $PrMn_2Ge_{0.8}Si_{1.2}$ over the temperature range 5-480 K. In addition to the 3 h data collection at each selected temperature, we performed short time data collection (10 min) during sample cooling to get more detailed information around the phase transitions.

Neutron diffraction patterns for $PrMn_2Ge_{1.0}Si_{1.0}$ at selected temperatures are shown in Fig. 8 with the temperature dependences of the intensities of the (101), (002) and (112) reflections shown in Fig. 9(a). The intensity of the (002) nuclear reflection remains effectively unchanged over the whole temperature as expected, with the phase transitions at T_N^{intra} ~ 424 K, T_C^{inter} ~ 311 K and T_C^{Pr} ~ 66 K clearly marked by changes in the intensities of the (101) and (112) reflections due to magnetic scattering. As shown in Fig. 9(b), the full width at half maximum (FWHM) for the (110) reflection increases significantly with decreasing temperature from FWHM~0.775° above ~200 K attaining FWHM>~0.795° before returning to a value of FWHM<~0.78° at low temperatures. The temperature at which the FWHM first broadens corresponds to the transition temperature T_N^{inter}~200 K at which the magnetization of $PrMn_2Ge_{1.0}Si_{1.0}$ decreases (Fig. 3(a)) and an antiferromagnetic state is expected. As indicated by the neutron diffraction pattern of $PrMn_2Ge_{1.0}Si_{1.0}$ at 100 K (Fig. 8), it is also found that in this region of broadened FWHM, the (111) peak appears while the (112) remains. According to neutron diffraction condition (3), the appearance of the (111) reflection peak at 100 K means the formation of the AF*mc* state while the remaining of (112) reflection indicates that the F*mc* state still exists at the same temperature based on neutron diffraction condition (2). This behaviour - the co-existence of (111) and (112) reflections at 100 K - indicates co-existence of two crystallographic states corresponding to the ferromagnetic F*mc* and antiferromagnetic AF*mc* states and is similar to the co-existence of magnetic phases first reported in RMn_2X_2 compounds for $La_{1-x}Y_xMn_2Si_2$ [16]. Refinements of the neutron diffraction

patterns confirm that in this region of broadened (110) reflections - from ~200 K to ~51 K (Fig. 9(b)) - both ferromagnetic and antiferromagnetic phases appear for $PrMn_2Ge_{1.0}Si_{1.0}$. For example, at 100 K, $PrMn_2Ge_{1.0}Si_{1.0}$ exhibits co-existence of 71±7% of the F*mc* phase and 29±6% of the AF*mc* phase (determined from refinements of the neutron diffraction patterns, see below). The Rietveld refinements also confirm that the unit cell for the AF*mc* phase is smaller than the unit cell for the *Fmc* phase (e.g. at 100 K, unit cell volume V=176.8±0.1 $Å^3$ for F*mc* while V= 174.5±0.1 $Å^3$ for AF*mc*). This agrees well with the behaviour detected in other re-entrant ferromagnetism system such as $NdMn_{2-x}Fe_xGe_2$ [19] and $SmMn_2Ge_2$ [20] where around 3% contraction of unit cell is observed when the magnetic state changes at T_N^{inter} from F*mc* to AF*mc* in $SmMn_2Ge_2$. As already noted, with decrease in temperature below T_C^{Pr}~51 K, the width of the (110) peak approaches the lower value FWHM<~0.78° as expected on reversion to a single phase state. In addition, from Figs 8 and 9, it can be seen that below T_C^{Pr}~51 K, the intensities of both the (101) and (112) peaks increase with decreasing temperature while the (111) peak has already disappeared (e.g. 50 K pattern in Fig. 8). This indicates that below T_C^{Pr}, the Pr-sublattice orders ferromagnetically and that the Mn-sublattice reverts to the F*mc* magnetic structure. Refinement of the lowest temperatures patterns confirm that below T_C^{Pr}, the Pr-sublattice orders with ferromagnetic Pr magnetic moments coupled parallel with Mn moments along the c-axis to form the combined F*mc*+F*(Pr)* phase region.

Since the magnetic moments, lattice parameters and the scale parameters of the AF*mc* and F*mc* phases within the region of phase co-existence are highly correlated, we adopt the similar approach described for the $La_{1-x}Y_xMn_2Si_2$ system ([16]; see also $La_{1-x}Pr_xMn_2Si_2$ [9]) with several parameters being constrained during the refinements in the co-existence region. The magnetic moments of Mn for the F*mc* component are directly derived from the temperature dependence of the Mn magnetic moments obtained from Rietveld refinements in the single phase regions (below T_C^{Pr} and above T_N^{inter} up to T_C^{inter}), we refine other parameters including magnetic moments for *AFmc* component and lattice parameters for both AF*mc* and F*mc* within the region of phase co-existence. Refinement of the neutron diffraction patterns in this two phase region leads to the *a* and

c lattice constants and the fractions of the F*mc* and AF*mc* phases. The structural and magnetic parameters of $PrMn_2Ge_{1.0}Si_{1.0}$ at selected temperatures are summarized in Table 1.

Fig. 10(a) shows a comprehensive set of diffraction patterns over the temperature range 20–300 K for $PrMn_2Ge_{0.8}Si_{1.2}$ with the temperature dependences of the intensities of the (111) and (112) reflections and the FWHM for the (110) reflection as derived from single peak fitting procedure with a Gaussian peak shape function shown in Figures 10(b) and (c). The behaviour of the (111) and (112) reflections for $PrMn_2Ge_{0.8}Si_{1.2}$ indicate that the F*mc* and AF*mc* magnetic phases coexist over the temperature range 20-300 K. However there are two significant differences between $PrMn_2Ge_{1.0}Si_{1.0}$ and $PrMn_2Ge_{0.8}Si_{1.2}$: first there is no separate F*mc* phase before the onset of the region of co-existence, and secondly the co-existence extends beyond T_C^{Pr}~54 K into the (F*mc* + F*(Pr)*) region for $PrMn_2Ge_{0.8}Si_{1.2}$ sample.

The temperature dependences of the structural and magnetic parameters as derived from the Rietveld refinements are listed in Tables 1 and 2. It can be seen that the lattice constants for the AF*mc* state are smaller than those for the F*mc* state in the co-existence region. This behaviour agrees with findings as discussed above [19, 20], and confirms our ability to separate the AF*mc* and F*mc* phases in the refinements.

3. $PrMn_2Ge_{0.4}Si_{1.6}$

The Mn-Mn intralayer distance for $PrMn_2Ge_{0.4}Si_{1.6}$ at room temperature has been derived to be $d_{Mn\text{-}Mn}$=2.865 Å (a=4.052 Å < a_{crit2}=4.06 Å). The $PrMn_2Ge_{0.4}Si_{1.6}$ is expected to exhibit the AF*mc* magnetic structure at room temperature. We have recorded neutron diffraction patterns at T=5 K, 76 K, 151 K, 249 K, 311 K, 349 K, 397 K, 466 K with selected patterns shown in Fig. 11(a). Refinements of the neutron diffraction patterns at 466 K and 349 K confirm that $PrMn_2Ge_{0.4}Si_{1.6}$ is paramagnetic and antiferromagnetic (intralayer AF*l*) at these temperatures respectively as expected (T_N^{intra}=371 K; Fig. 5(a)). Refinement of the neutron diffraction pattern at 311 K yields a canted antiferromagnetic AF*mc* structure with canting angle θ=60(±1.8)° which agrees well with

expectation based on the lattice parameters. As in Figure 11(b), diffraction features associated with the various magnetic states can be seen by the intensity changes of the (101) and (111) reflections; in particular a marked increase in the intensity of the (111) reflection is noted around ~29 K while the intensity of the (101) reflection decreases, indicating that the canting angle θ increases around ~29 K. This change of canting angle of Mn moment at 29 K may be responsible for the anomaly in M-T curve at lower temperature (see Fig. 5(a)).

The lattice constants and Mn magnetic moments for $PrMn_2Ge_{1.6}Si_{0.4}$ are shown in Fig. 12. The *a* and *c* parameters derived from the peak positions based on neutron patterns collected on cooling are also shown - good agreement is obtained with data from the patterns measured under thermally static conditions. As can be seen from the structural and magnetic data of Figures 12(b) and 12(c), the appearance of component μ_c^{Mn} of the Mn moment along the c-axis at T_N^{inter}, leads to a significant contribution to the thermal expansion with a pronounced anomaly in the c/a axial ratio at T_N^{inter}. This behaviour is similar to that noted above for $PrMn_2Ge_{1.6}Si_{0.4}$.

The refinements reveal that the AF*mc* magnetic structure remains unchanged as the temperature decreases from 311 K down to 5 K. This leads to the graph of canting angle θ of the Mn moment from T_N^{inter}~333 K to 5 K as shown in the insert to Fig. 12(c) (T_N^{inter} is the temperature at which the AF*l* structure of effective canting angle θ=90° transforms to the AF*mc* structure). Given the anomaly in the magnetisation versus temperature curve of Fig. 5(a) at T_{sr}~282 K and the relatively abrupt change in the canting angle θ at ~282 K (arrow in the insert of Fig. 12(c)), we conclude that the magnetic anomaly at ~282 K is associated with a spin reorientation temperature T_{sr}. However, the anomaly at T_{sr}~282 K could also indicate coexistence of antiferromagnetic and weak ferromagnetic components below 282 K similar to the behaviours observed in $PrMn_2Ge_{1.0}Si_{1.0}$ and $PrMn_2Ge_{0.8}Si_{1.2}$ as outlined above. However within statistical resolution, there is no evidence in the neutron diffraction patterns for a ferromagnetic component to the patterns below T_{sr}~282 K. Similar behaviour - where weak ferromagnetic components of the ordered Mn moments (around T_C=240 K) are clearly detected in magnetization measurements but cannot be determined from

powder neutron diffraction - has been found for $PrMn_2Si_2$ [9]. This behaviour was attributed to the assumption that the small ferromagnetic component in $PrMn_2Si_2$ was too small for detection by neutron scattering [9]. At 5 K, the values of Mn magnetic moments derived for $PrMn_2Ge_{0.4}Si_{1.6}$ are μ_c^{Mn}= 1.95 μ_B, μ_{ab}^{Mn}= 1.12 μ_B and μ_{tot}^{Mn}= 2.25 μ_B with the canting angle being θ=30(±0.6)°.

4. Discussion

The ground state values (base temperatures ~5 K) of the total magnetic moment μ_{tot}^{Mn} and basal plane moment μ_{ab}^{Mn} of $PrMn_2Ge_{2-x}Si_x$ compounds decrease with increasing Si content. This behaviour indicates that contraction of the unit cell leads to a reduction in the Mn moment value (e.g. μ_{tot}^{Mn} = 3.16(±0.07) μ_B for x=0.4; μ_{tot}^{Mn} =2.25(±0.02) μ_B for x=1.6) and agrees well with the tendency detected for both RMn_2Si_2 and RMn_2Ge_2 systems where both μ_{tot}^{Mn} and μ_{ab}^{Mn} are found to decrease with decrease in lattice constant *a*. The moment values also agree with typical values for the RMn_2Si_2 and RMn_2Ge_2 systems - μ_{tot}^{Mn} ~ 2-2.4 μ_B for RMn_2Si_2 compounds (e.g. μ_{tot}^{Mn} = 2.43 μ_B in $LaMn_2Si_2$ [21]) and μ_{tot}^{Mn} ~ 2.4–3.3 μ_B for RMn_2Ge_2 compounds (e.g. μ_{tot}^{Mn} = 3.06 μ_B in $LaMn_2Ge_2$ [21]) .

First-principles calculations on $LaMn_2Ge_2$ and $LaMn_2Si_2$ [21] suggested that the reduction of Mn moments in $LaMn_2Si_2$ (a=4.11 Å) compared with $LaMn_2Ge_2$ (a=4.19 Å), depends primarily on the Mn-Mn distances (stronger Mn-Mn hybridization due to shorter Mn-Mn distance leads to a smaller local Mn moment [22]) but that the larger hybridization strength of Si-Mn in $LaMn_2Si_2$ than Ge-Mn in $LaMn_2Ge_2$ also plays a role. Similarly, the reduction of Mn moments in the present $PrMn_2Ge_{2-x}Si_x$ system with increasing Si content can be ascribed to these two factors: (1) decrease of the Mn-Mn spacing (at 300 K, d_{Mn-Mn} = 2.916 Å for $PrMn_2Ge_2$; d_{Mn-Mn} = 2.845 Å for $PrMn_2Si_2$) and (2) increase of Si-Mn hybridization strengths compared with Ge-Mn hybridization [22]. The current investigation has also revealed that the moment of Pr sublattice increases from 1.52(±0.04) μ_B for x=0.4 to 2.06(±0.03) μ_B for x=1.2 and that Pr atoms do not carry a magnetic moment for Si contents x≥1.6.

The temperature dependence of the $PrMn_2Ge_{2-x}Si_x$ lattice parameters demonstrate that an anomaly in thermal expansion is accompanied with the appearance of the interlayer Mn–Mn interactions. This behaviour agrees well with our previous conclusion based on $PrMn_{2-x}Fe_xGe_x$ where we found that the interlayer Mn-Mn interactions rather than the intralayer Mn-Mn interactions play the major role in the anomalous thermal expansion [6, 14]. Combining the present findings with the magnetic results of Kervan *et al.* [10] has enabled us to construct the magnetic phase diagram for the $PrMn_2Ge_{2-x}Si_x$ system shown in Figure 13. The majority of the boundary lines separating the different magnetic phases are well defined by the density of available data points, with extrapolations based on the trends of the current data of two boundaries (F*mc* to F*mi*; AF*l* to F*mc*) indicated as dotted lines. The shaded region in Figure 13 indicates the region of co-existence of the F*mc* and AF*mc* phases; we have also made a theoretical extension for the phase boundary of co-existence range based on the phase fraction for $PrMn_2Ge_{2-x}Si_x$ with x=1.0 and 1.2 [23]. Given that the magnetic states depend sensitively on the Mn-Mn distances in this system, the co-existence of magnetic states is considered to be related to the non-random variation of site concentrations of Si and Ge, leading in turn to differences on the local environments throughout the sample [23].

Figure 13 demonstrates that the magnetic states at room temperature have been modified by Si substitution due to the contraction of unit cell as expected. Samples with x>~1.5 where the lattice constant *a* is below a_{crit1}=4.06 Å (Fig. 1) are antiferromagnetic at room temperature with no ferromagnetic order evident over the entire temperature range, whereas samples of Si content x <~1.0 are ferromagnetic at room temperature. It is interesting to note that samples with Si concentrations in the range x~1.0-1.5 (where lattice constant *a* crosses the threshold value of a_{crit1}=4.06 Å), corresponds approximately to the region of co-existence of the AF*mc* and F*mc* phases around room temperature. Given that a compound has a smaller unit cell in an antiferromagnetic state than in a ferromagnetic state, the deviation from the linear behaviour in the composition dependence of lattice constants at room temperature (Fig. 1) can be understood in

terms of the difference in magnetic states at room temperature for these samples. This behaviour in turn reflects the larger contribution from magnetism to thermal expansion [14].

It can be seen from Figure 13 that compounds with Si content x≥1.6 have a relatively simple magnetic behaviour, transforming from paramagnetism at high temperatures to AF*l* followed by *AFmc* with decreasing temperature with no evidence of ordering of the Pr-sublattice. By comparison, Ge-rich samples (x<0.8) successively exhibit four magnetic states – AF*l*, F*mc*, F*mi*, F*mi*+F*(Pr)* - on cooling from the high temperature paramagnetic phase. Figure 13 also indicates that the F*mi* structure only occurs for Si content x <~0.8. This is reflected by the decrease in wave vector with Si content from q_c = 0.28 for $PrMn_2Ge_2$ at 2 K to q_c = 0.23 for $PrMn_2Ge_{1.6}Si_{0.4}$ at 5 K. Similar behaviour has been detected in the $PrMn_{2-x}Fe_xGe_2$ [14] and $Pr_{1-y}Lu_yMn_2Ge_2$ [2] systems where the absence of F*mi* is found at x< 0.38 and y<0.4, respectively.

As also evident from the phase diagram, re-entrant ferromagnetism is obtained for $PrMn_2Ge_{2-x}Si_x$ in the intermediate Si concentration range 0.95 <x <1.5. Different from other re-entrant ferromagnetism systems such as $PrMn_{1.4}Fe_{0.6}Ge_2$ [6, 14], $SmMn_2Ge_2$ [15], $Nd_{0.35}La_{0.65}Mn_2Si_2$ [24], $NdMn_{1.575}Fe_{0.425}Ge_2$ [10], $Pr_{0.5}Y_{0.5}Mn_2Ge_2$ [25], the co-existence of magnetic states F*mc* and AF*mc* has been shown to occur for both the $PrMn_2Ge_{1.0}Si_{1.0}$ and $PrMn_2Ge_{0.8}Si_{1.2}$ compounds. This co-existence reflects the incompleteness of phase transition from F*mc* to AF*mc* with decreasing temperature. The incomplete nature of the phase transition in these compounds may be responsible for the relatively low magnetocaloric entropy change around T_C^{Pr} obtained for $PrMn_2Ge_{0.8}Si_{1.2}$ [10]. Moreover, it also can be concluded from Fig. 13 that Pr ordering only exists with the presence of the F*mc* or F*mi* phases at low temperature, thus indicating that the ferromagnetic ordering of the Pr-sublattice is always accompanied with the presence of Mn-sublattice ferromagnetic ordering in these systems.

5. Conclusions

The effects of replacing Ge with the smaller Si atoms in $PrMn_2Ge_{2-x}Si_x$ on the structural and magnetic properties have been investigated by X-ray diffraction, magnetic, differential scanning

calorimetry and neutron diffraction measurements over the temperature range 5 K to 480 K and the magnetic phase diagram constructed. Replacement of Ge by Si leads to a significant contraction of the unit cell; the non-linear behaviour detected in the composition dependence of lattice constants at room temperature reflects the strong magnetovolume effects.

The overall magnetic behaviour of $PrMn_2Ge_{2-x}Si_x$ is governed by the strong dependence of the magnetic couplings between and, particularly, within the Mn layers. Compounds with low ($x \leq 0.9$) and high levels ($x \geq 1.6$) of Si content exhibit magnetic behaviour similar to the end products $PrMn_2Ge_2$ and $PrMn_2Si_2$. By comparison, both $PrMn_2Ge_{1.0}Si_{1.0}$ and $PrMn_2Ge_{0.8}Si_{1.2}$ show re-entrant ferromagnetic behaviour as the structural and magnetic interplay takes place on replacement of Ge with Si. Coexistence of magnetic states AF*mc* and F*mc* has been detected for both $PrMn_2Ge_{1.0}Si_{1.0}$ and $PrMn_2Ge_{0.8}Si_{1.2}$ with the unit cell volume of the F*mc* state found to be larger than the AF*mc* state.

The Mn sublattice exhibits magnetic ordering over the entire concentration range, whereas the Pr sublattice orders ferromagnetically for Si contents $x<\sim1.5$. Values of the ground state Mn magnetic moments decrease with increasing Si content due to the reduction of Mn-Mn separation distance and stronger Si-Mn hybridization compared with Ge-Mn hybridization.

Acknowledgments

The work is supported in part by grants from the Australian Research Council Discovery Projects (DP0879070; DP110102386) and the Australian Research Council LIEF Grant (LE0775559). We also acknowledge financial support from the Access to Major Research Facilities Programme, which is a component of the International Science Linkages Programme established under the Australian Government's innovation statement, Backing Australia's Ability. The authors acknowledge the assistance of Drs A.J. Studer and M. Avdeev during experiments at OPAL.

References

[1] A. Szytula, In: K.H.J. Buschow (Ed.), Handbook of Magnetic Materials. Vol. 6, Elsevier, Amsterdam, 1991, p. 85.

[2] J.L.Wang, S. J. Campbell, A.J. Studer, M. Avdeev, R. Zeng and S X Dou, J. Phys.: Condens. Matter **21**, 124217 (2009) and references therein

[3] M. Hofmann, S.J. Campbell and A.V.J. Edge, Phys. Rev. B **69**, 174432 (2004); J. L. Wang, S. J. Campbell, J. M. Cadogan, A. J. Studer, R. Zeng, and S. X. Dou, Applied Physics Letters **98,** 232509 (2011).

[4] P. Kumar, K.G. Suresh, A.K. Nigam, A. Magnus, A.A. Coelho and S. Gama, Phys. Rev. B **77**, 224427 (2008)

[5] M Hofmann, S J Campbell, K Knorr, S Hull and V. Ksenofontov, J Applied Physics **91,** 8126 (2002)

[6] J.L. Wang, S.J. Campbell, J.M. Cadogan, O. Tegus, A.J. Studer and M. Hofmann, J. Phys.: Condens. Matter **18**, 189 (2006); J.L. Wang, A.J. Studer, S.J. Campbell, M Hofmann, and J.M. Cadogan, Physica B **385–386,** 326 (2006).

[7] I. Nowik, Y. Levi, I. Felner and E.R. Bauminger. J. Magn. Magn. Mater. **147,** 373 (1995)

[8] R. Welter, G. Venturini, D. Fruchard and B. Malaman, J. Alloys Compd. **191,** 263 (1993)

[9] I. Dincer, Y. Elerman, A. Elmali, H. Ehrenberg, and G. André, J. Magn. Magn. Mater. **313**, 342 (2007)

[10] S Kervan, A Kilic and A Gencer, J. Phys.: Condens. Matter **16**, 4955 (2004)

[11] J. L. Wang, S. J. Campbell, A. J. Studer, M. Avdeev, M. Hofmann, M. Hoelzel, and S. X. Dou, J. Appl. Phys. **105**, 07A909 (2009)

[12] K A Gschneidner Jr, V K Pecharsky and A O Tsokol, Rep. Prog. Phys. 68 1479 (2005); D. Haskel, Y. B. Lee, B. N. Harmon, Z. Islam, J. C. Lang, G. Srajer, Ya. Mudryk, K. A. Gschneidner, Jr., and V. K. Pecharsky, Phys. Rev. Lett. **98**, 247205 (2007)

[13] J. Rodriguez-Carvajal, "FULLPROF: A program for Rietveld Refinement and Pattern Matching Analysis," Abstracts of the Satellite Meeting on Powder Diffraction of the XV Congress of the International Union of Crystallography, Toulouse, France, 1990 _unpublished_, p. 127; http://www-llb.cea.fr/fullweb/

[14] J.L. Wang, S.J. Campbell, A.J. Studer, M. Avdeev, M. Hofmann, M. Hoelzel and S.X. Dou, J. Appl. Phys. **104**, 103911 (2008);

[15] H. Fujii, T. Okamoto, T. Shigeoka and N. Iwata, Solid State Comm. **53**, 715 (1985);

[16] M. Hofmann, S.J. Campbell and S.J. Kennedy, J. Phys.: Condens. Matter **12**, 3241(2000)

[17] A. Arrott, Phys. Rev. **108,** 1394 (1957)

[18] J. L. Wang, S. J. Campbell, M. Hofmann, S. J. Kennedy, M Avdeev, M. F. Md Din, R. Zeng, Z. X. Cheng and S. X. Dou, J. Appl. Phys. 113, 17E147 (2013)

[19] G. Venturini, B. Malaman and E. Ressouche, J. Alloys Compd. **237,** 61 (1996)

[20] M. Duraj, R. Duraj, A. Szytula and Z. Tomkowicz, J. Magn. Magn. Mater. **73,** 240 (1988)

[21] S. Di Napoli, A. M. Llois, G. Bihlmayer, S. Blügel, M. Alouani, and H. Dreyssé, Phys. Rev. B **70**, 174418 (2004).

[22] R. Welter, G. Venturini, E. Ressouche and B. Malaman**,** J. Alloys Compd. **218**, 204 (1995)

[23] J. L. Wang, S. J. Kennedy, S. J. Campbell, M. Hofmann and S. X. Dou, Phys. Rev. B **87**, 104401 (2013)

[24] G. Venturini, R. Welter, E. Ressouche and B. Malaman, J. Magn. Magn. Mater. **150,** 197 (1995) and references therein

[25] J. L. Wang, L. Caron, S. J. Campbell, S. J. Kennedy, M. Hofmann, Z. X. Cheng, M. F. Md Din, A. J. Studer, E. Brück, and S. X. Dou, Phys. Rev. Lett. **110** (2013) 217211

Figure captions

Fig. 1 (Color online) Composition dependence of (a) lattice constants *a* and *c*, (b) *c/a* ratio and (c) unit cell volume V for $PrMn_2Ge_{2-x}Si_x$ at room temperature. The arrows indicate the region where the slope changes. The lines are guides to the eye**.**

Fig. 2 (Color online) Composite figures showing the temperature dependent magnetization obtained on cooling $PrMn_2Ge_{1.6}Si_{0.4}$ in a field of *B*=0.01 T (left region) and the DSC results (right region). The transition temperatures are indicated by arrows. The inset to Figure 2 shows the *dM*/*dT* versus *T* plot as an example of how T_C^{Pr} and $T_{c/c}$ were determined.

Fig. 3 (Color online) Composite figure showing the temperature dependent magnetization obtained on cooling $PrMn_2Ge_{1.0}Si_{1.0}$ in a field of *B*=0.01 T (left part) and the DSC results (right part). The transition temperatures are indicated by arrows.

(b) Thermomagnetic curves obtained at different temperatures and applied fields for $PrMn_2Ge_{0.8}Si_{1.2}$ plotted as three dimensional M-B-T surface curves. The transition temperatures T_C^{Pr}, T_N^{inter} and T_C^{inter} are marked by arrows.

Fig. 4 (Color online) Magnetization measurements for $PrMn_2Ge_{0.8}Si_{1.2}$.

(a) Field dependence of the magnetization at T=10 K, 120 K, 250 K and 340 K and

(b) the corresponding Arrott plots of M^2 versus B/M. The insert to Fig 4(b) shows the dM/dB versus B curve at 120 K, indicating how the critical field value B_{cr} (marked by the vertical arrow) was determined.

(c) Temperature dependence of the critical magnetic field B_{cr} of the metamagnetic transition.

Fig. 5 (Color online) Composite figure showing the temperature dependent magnetization obtained on cooling $PrMn_2Ge_{0.4}Si_{1.6}$ in a field of *B*=0.01 T (left part) and the DSC results (right part) for: (a) $PrMn_2Ge_{0.4}Si_{1.6}$ and (b) $PrMn_2Si_2$. The transition temperatures are indicated by arrows.

Fig. 6 (Color online) Neutron diffraction patterns and Rietveld refinements for $PrMn_2Ge_{1.6}Si_{0.4}$ at 480 K, 340 K, 292 K, 150 K and 5 K (λ = 2.44 Å, E6 diffractometer, BENSC).

Fig. 7 (Color online) Temperature dependences of: (a) lattice constants *a* and *c*, (b) unit cell volume *V* and axial ratio *c/a*, and (c) magnetic moments for $PrMn_2Ge_{1.6}Si_{0.4}$. The transition temperatures are indicated by arrows. The insert to Figure 7(c) shows the canting angle of the Mn moment with respect to the c-axis.

Fig. 8 (Color online) Neutron diffraction patterns and Rietveld refinements for $PrMn_2Ge_{1.0}Si_{1.0}$ at 459 K, 316 K, 293 K, 100 K, 50 K and 5 K (λ = 2.44 Å, E6 diffractometer, BENSC).

Fig. 9 (Color online) Temperature dependences of: (a) the intensities of the (101), (002) and (112) reflections, and (b) the full width at half maximum (FWHM) of the (110) reflection for $PrMn_2Ge_{1.0}Si_{1.0}$.

Fig. 10 (Color online) (a) Representative neutron diffraction patterns for $PrMn_2Ge_{0.8}Si_{1.2}$ over the temperature range 20–300 K at 20 K intervals, (b) Temperature dependences of the intensities of the (111) and (112) reflections, and (c) the full width at half maximum (FWHM) of the (110) reflection for $PrMn_2Ge_{0.8}Si_{1.2}$

Fig. 11 (Color online) (a) Neutron diffraction patterns and Rietveld refinements for $PrMn_2Ge_{0.4}Si_{1.6}$ at 466 K, 349 K and 5 K (λ = 2.44 Å E6 diffractometer, BENSC).

(b) Temperature dependences of the intensities of the (101) and (111) reflections.

Fig. 12 (Color online) Temperature dependences of: (a) lattice constants *a* and *c*, (b) unit cell volume and axial ratio *c/a* and (c) magnetic moments for $PrMn_2Ge_{1.6}Si_{0.4}$ as derived from refinements of the neutron patterns (E6 diffractometer, BENSC). The smaller symbols in Fig. 12(a) represent the data derived from the corresponding peak positions obtained from ramp data on cooling as discussed in the text. The insert to Fig. 12(c) shows the temperature dependence of the canting angle θ for the Mn magnetic moment with respect to the c-axis. The open symbols in Fig. 12(a) show the data obtained on the Wombat diffractometer, OPAL.

Fig. 13 (Color online) The magnetic phase diagram of $PrMn_2Ge_{2-x}Si_x$ as a function of Si concentration *x*. The full symbols show data from references [9, 10]. The boundary separating the F*mi* and F*mc* phases has been extrapolated (dotted line) into the region of combined

ferromagnetic ordering for the Mn and Pr sublattices. The smaller symbols stand for the theoretical extension for the phase boundary of the co-existence range based on the phase fractions for $PrMn_2Ge_{2-x}Si_x$ with x=1.0 and 1.2.

Table 1 Structural and magnetic parameters derived from Rietveld refinements of the neutron diffraction patterns for $PrMn_2Ge_{1.0}Si_{1.0}$ compound. The errors are shown for the 5 K data as an example.

T (K)	5 K	100 K	100 K	200 K	302 K	410 K	460 K
Magnetic state	F*mc*+F(Pr)	28(6)% AF*mc*	72 (8)% F*mc*	F*mc*	F*mc*	AF*l*	PM
a (Å)	4.0616(5)	4.0477	4.0663	4.0670	4.0720	4.0777	4.0810
c (Å)	10.6780(13)	10.6516	10.6919	10.6911	10.7082	10.7338	10.7453
z_{Ge}	0.3827 (3)	0.3823	0.3823	0.3821	0.3824	0.3829	0.3824
μ_{ab} (μ_B)	2.19 (6)	2.04	1.84	1.88	1.58	0.95	-
μ_c (μ_B)	2.08 (5)	1.54	2.00	1.49	0.62	-	-
Canting angle	46.5	52.8	42.6	51.6	68.3	90	-
μ_{total} (μ_B)	3.02 (7)	2.56	2.72	2.40	1.70	0.95	-
μ_{Pr} (μ_B)	1.87 (4)	-	-	-		-	-
R_{wp}	3.87	3.51		3.46	3.10	3.50	3.66
R_{exp}	2.09	2.06		2.08	2.10	2.11	2.12

Table 2 Structural and magnetic parameters derived from Rietveld refinements of the neutron diffraction patterns for $PrMn_2Ge_{0.8}Si_{1.2}$. The errors were derived from the data fits with typical errors shown for the 5 K data.

T (K)	5 K	140 K	140 K	240 K	240 K	360 K	480 K
Magnetic state	Fmc+F(Pr)	72(3)% AF*mc*	28% F*mc*	36 (3.9)% AF*mc*	64(4.4)% F*mc*	AF*l*	PM
a (Å)	4.0570(4)	4.0511	4.06382	4.0512	4.0722	4.0719	4.0781
c (Å)	10.6589(10)	10.6699	10.67863	10.6479	10.6997	10.7004	10.7226
z_{Ge}	0.3823(2)	0.3820	0.3820	0.3823	0.3823	0.3825	0.3829
μ_{ab} (μ_B)	2.15 (6)	1.34	2.05	1.40	1.75	1.09 (3)	-
μ_c (μ_B)	1.85 (5)	1.79	1.68	1.14	1.43	-	-
Canting angle	49.2	48.5	50.7	50.7	58.2	90	
μ_{total} (μ_B)	2.84 (7)	2.24	2.65	1.81	2.26	1.09 (3)	-
μ_{Pr} (μ_B)	2.06 (3)	-	-	-		-	-
R_{wp}	3.82	2.98		2.83		3.72	3.64
R_{exp}	1.24	1.22		1.22		2.04	2.06

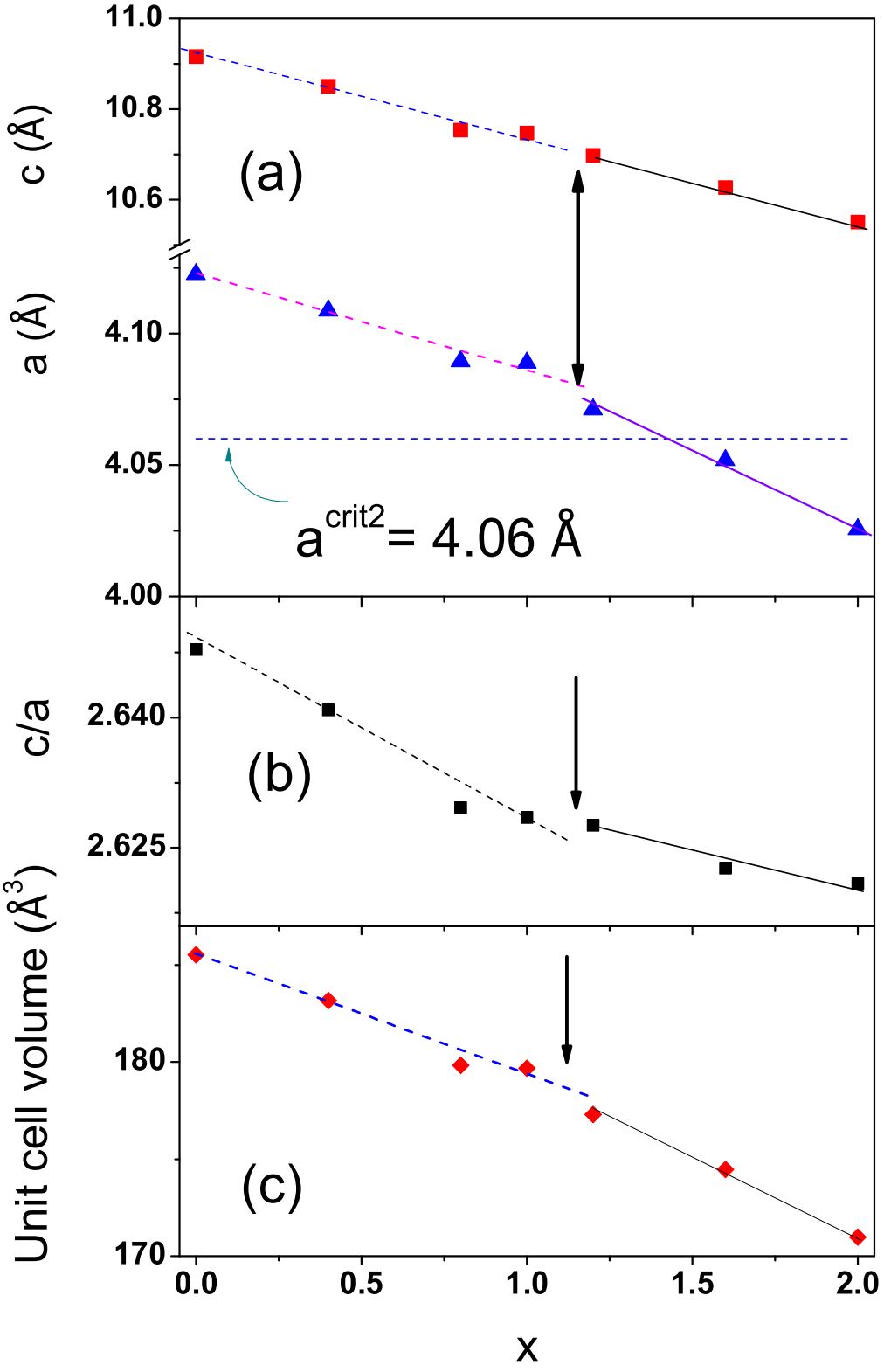

Figure 1 (figure1abc.eps)

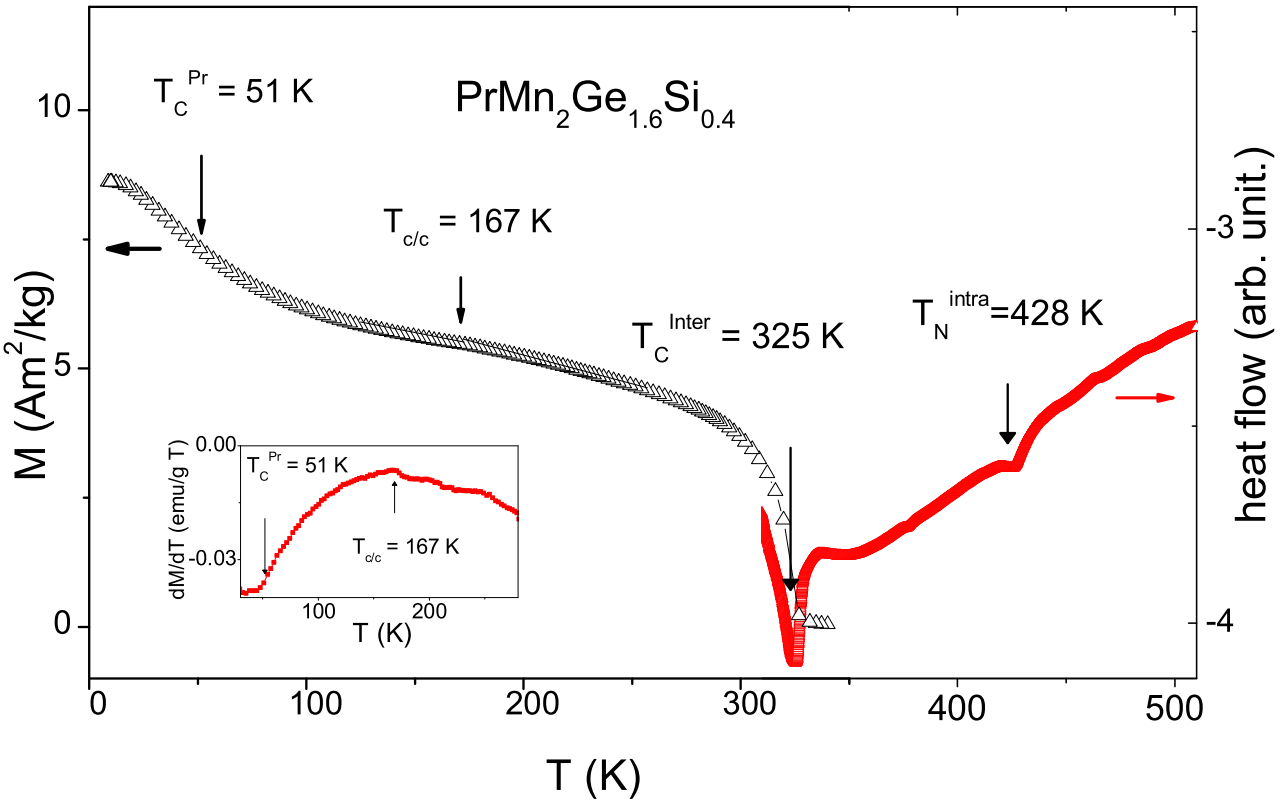

Figure 2 (figure2.eps)

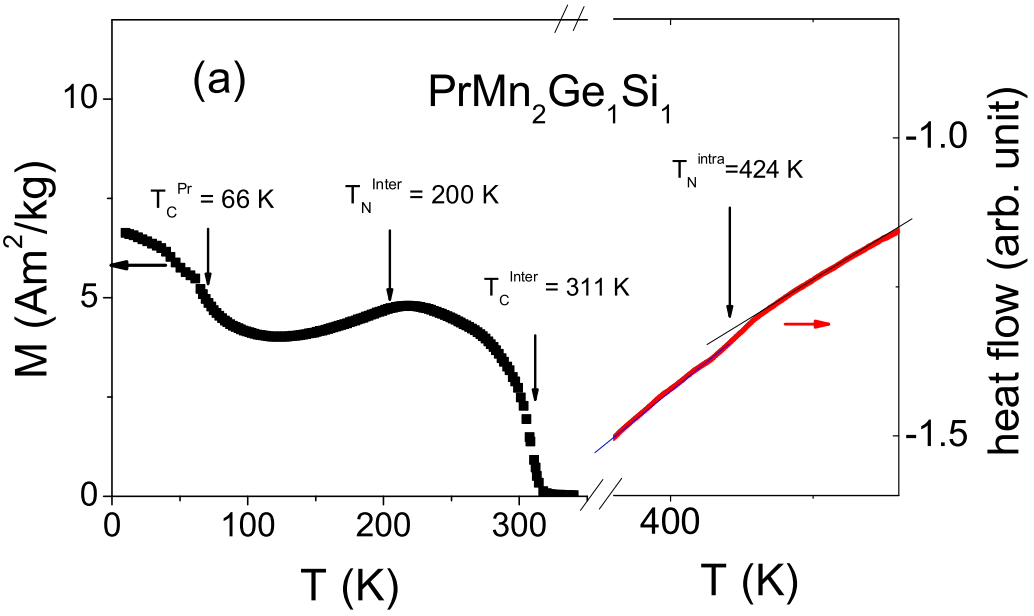

Figure 3a (figure3a.eps)

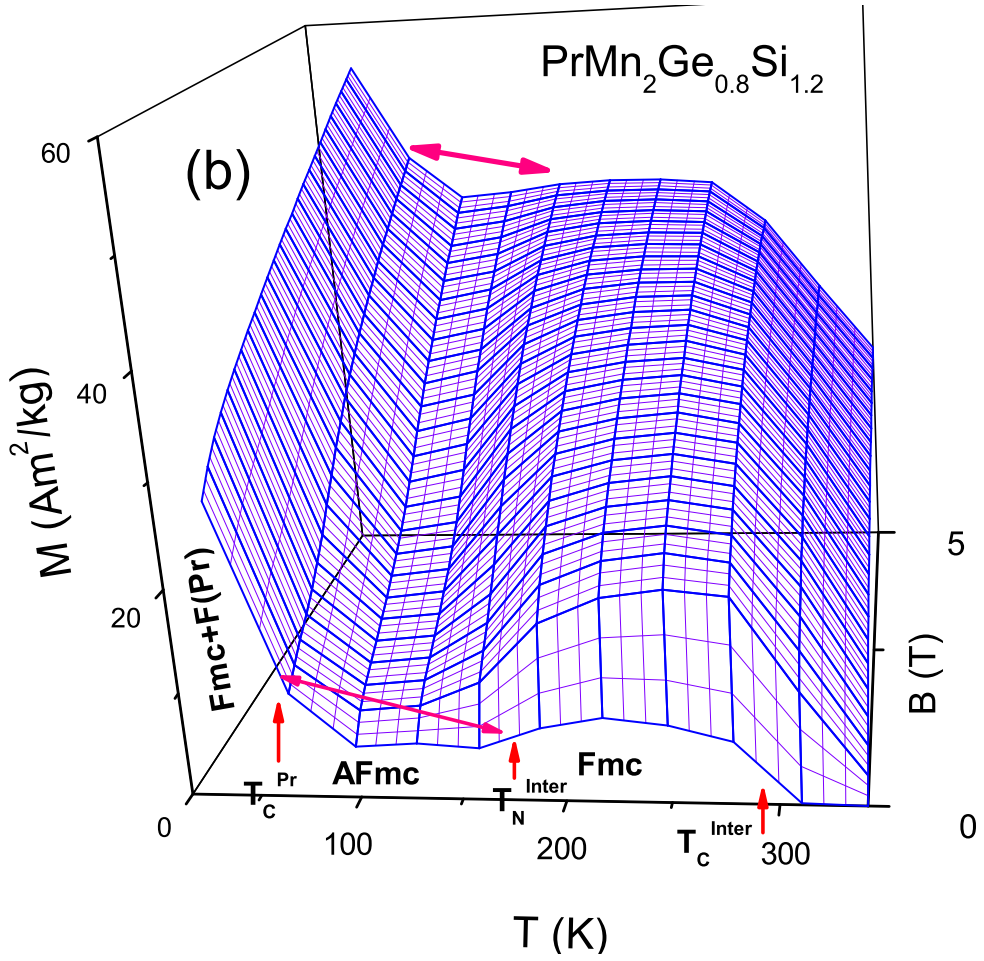

Figure 3b (figure3b.eps)

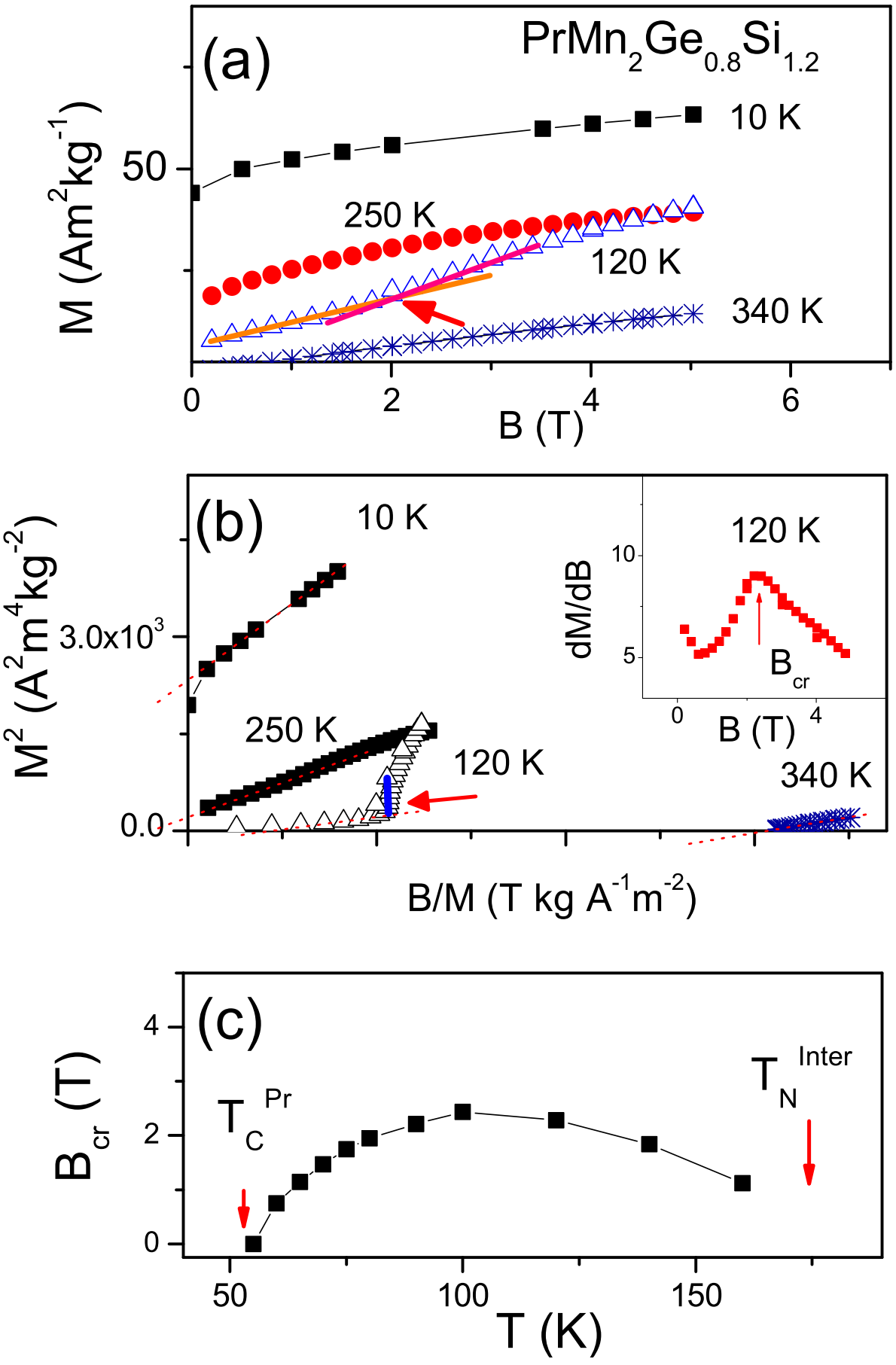

Figure 4 (figure4abc.eps)

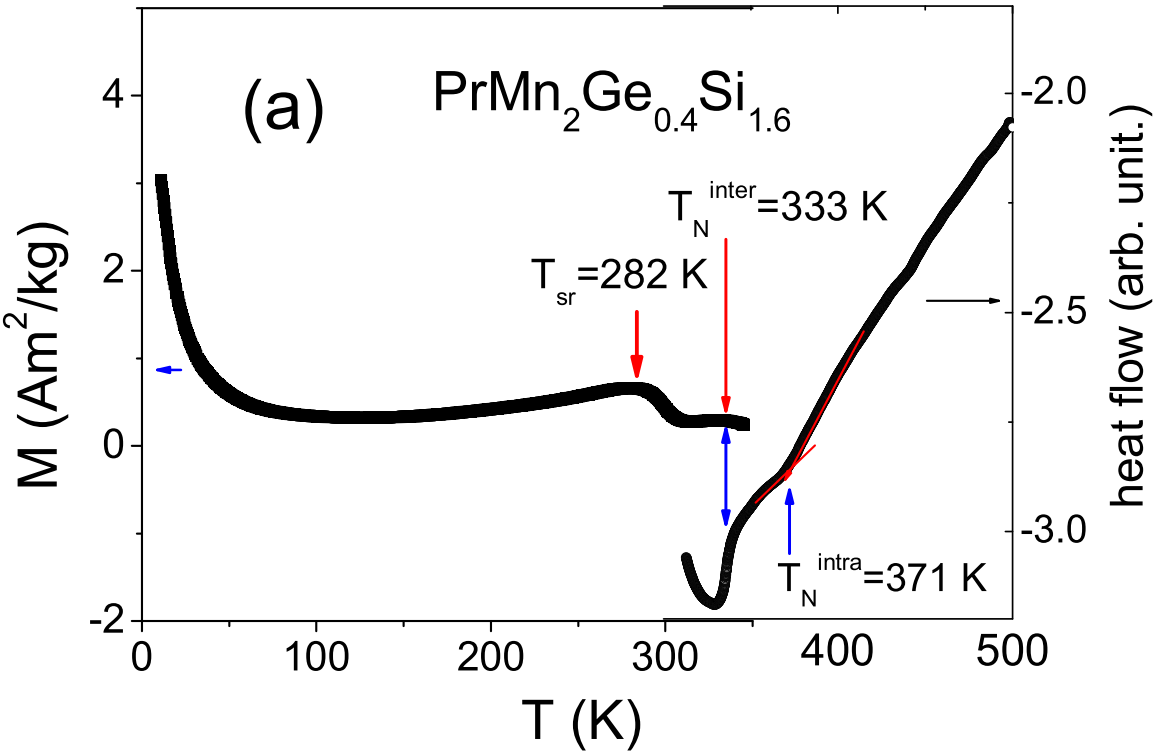

Figure 5a (figure5a.eps)

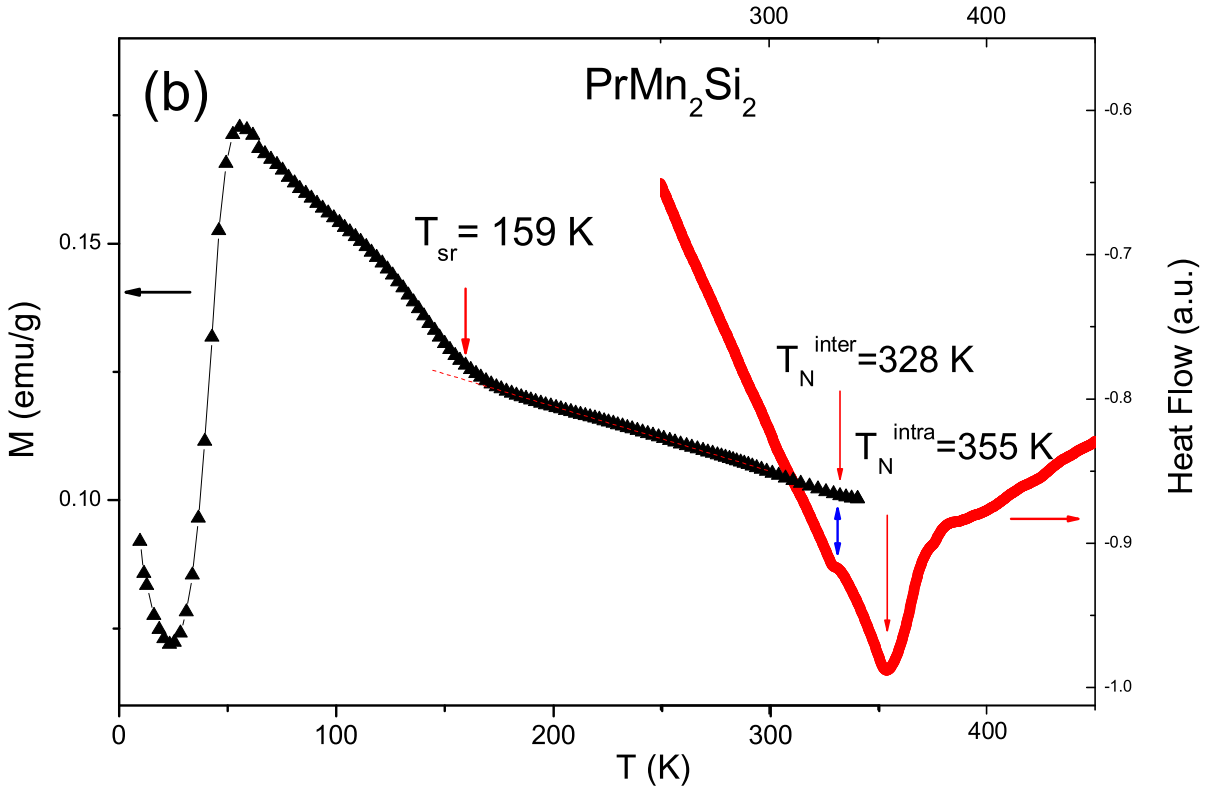

Figure 5b (figure5b.eps)

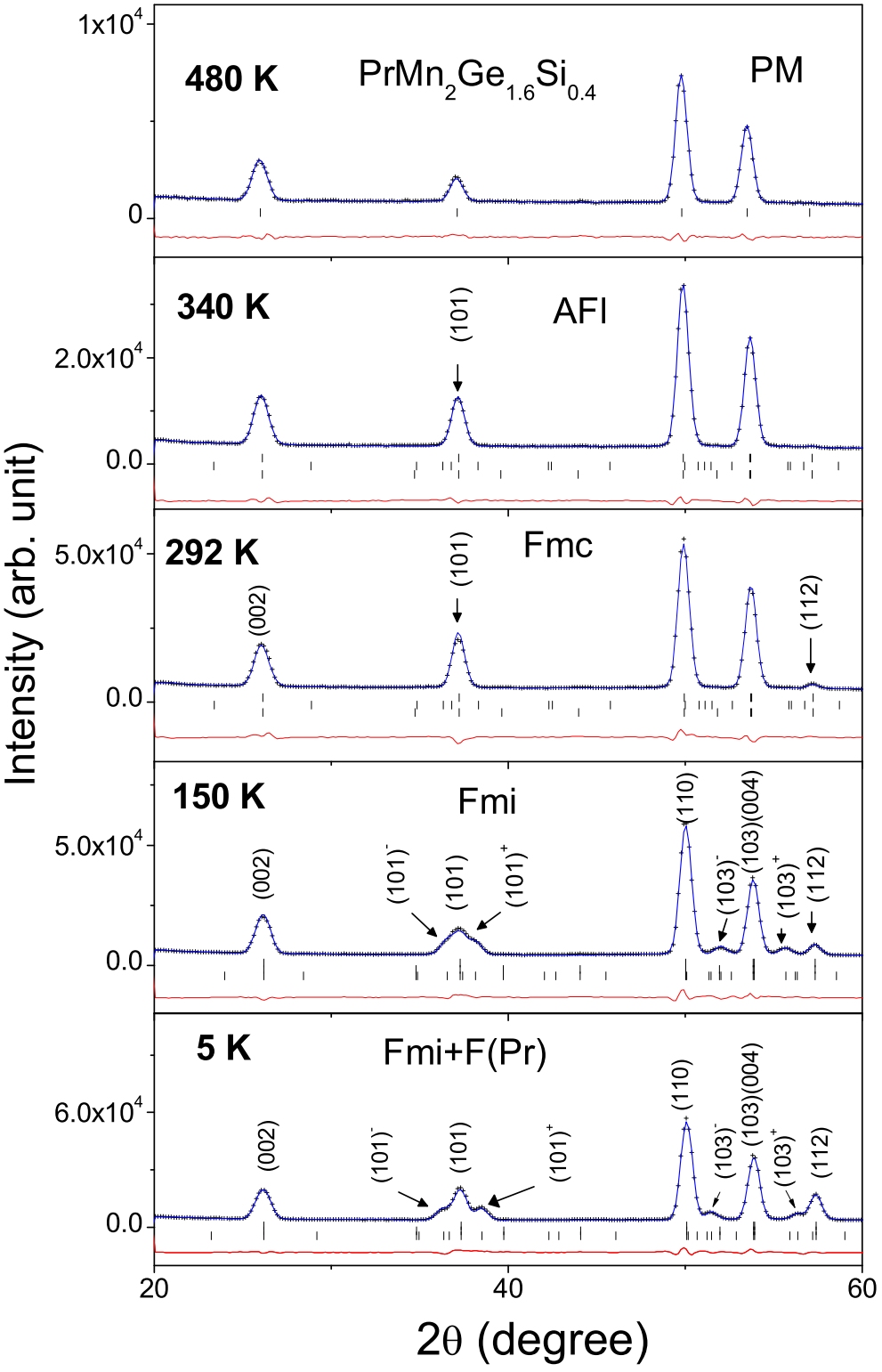

Figure 6 (figure6.eps)

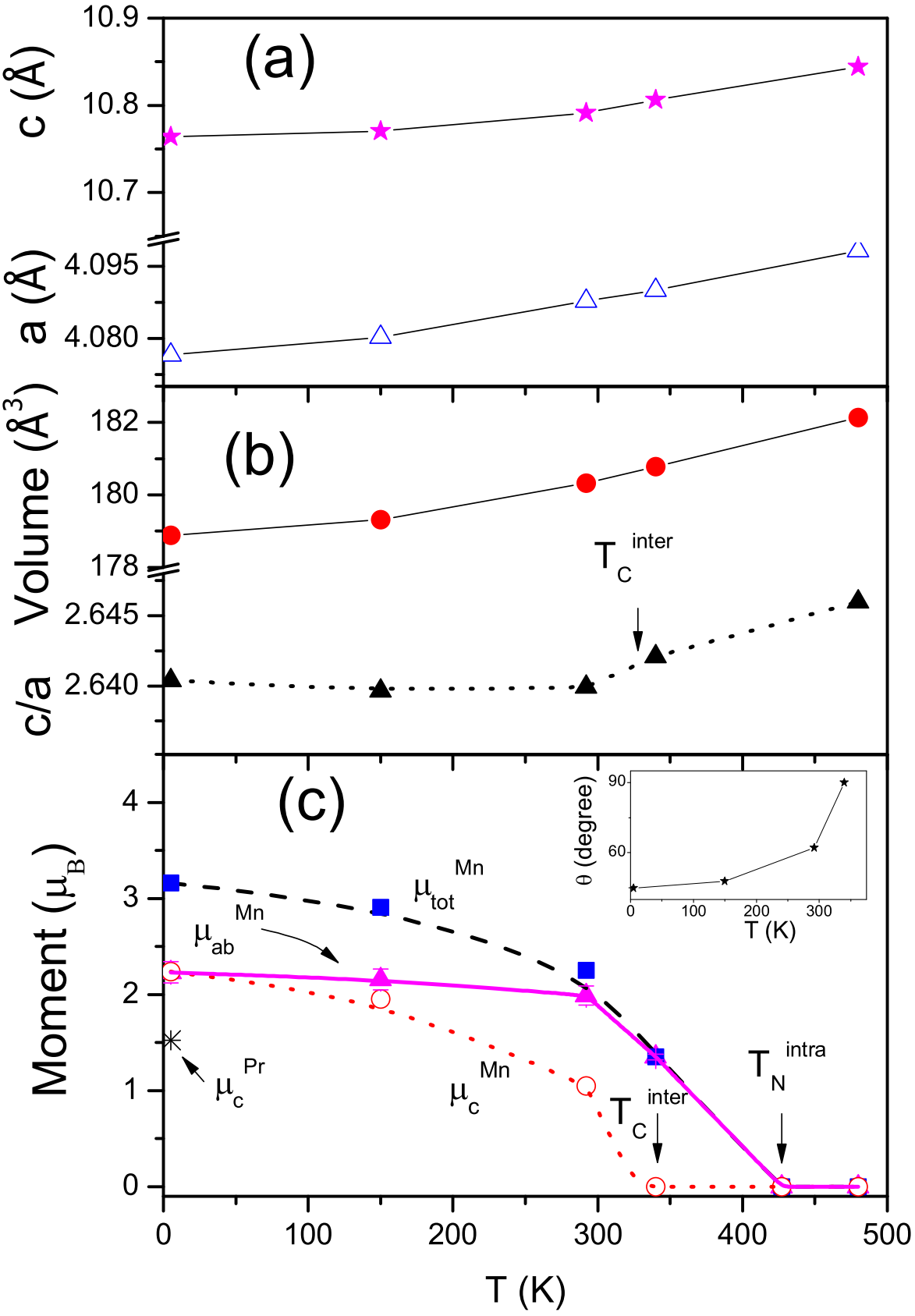

Figure 7 (figure7abc.eps)

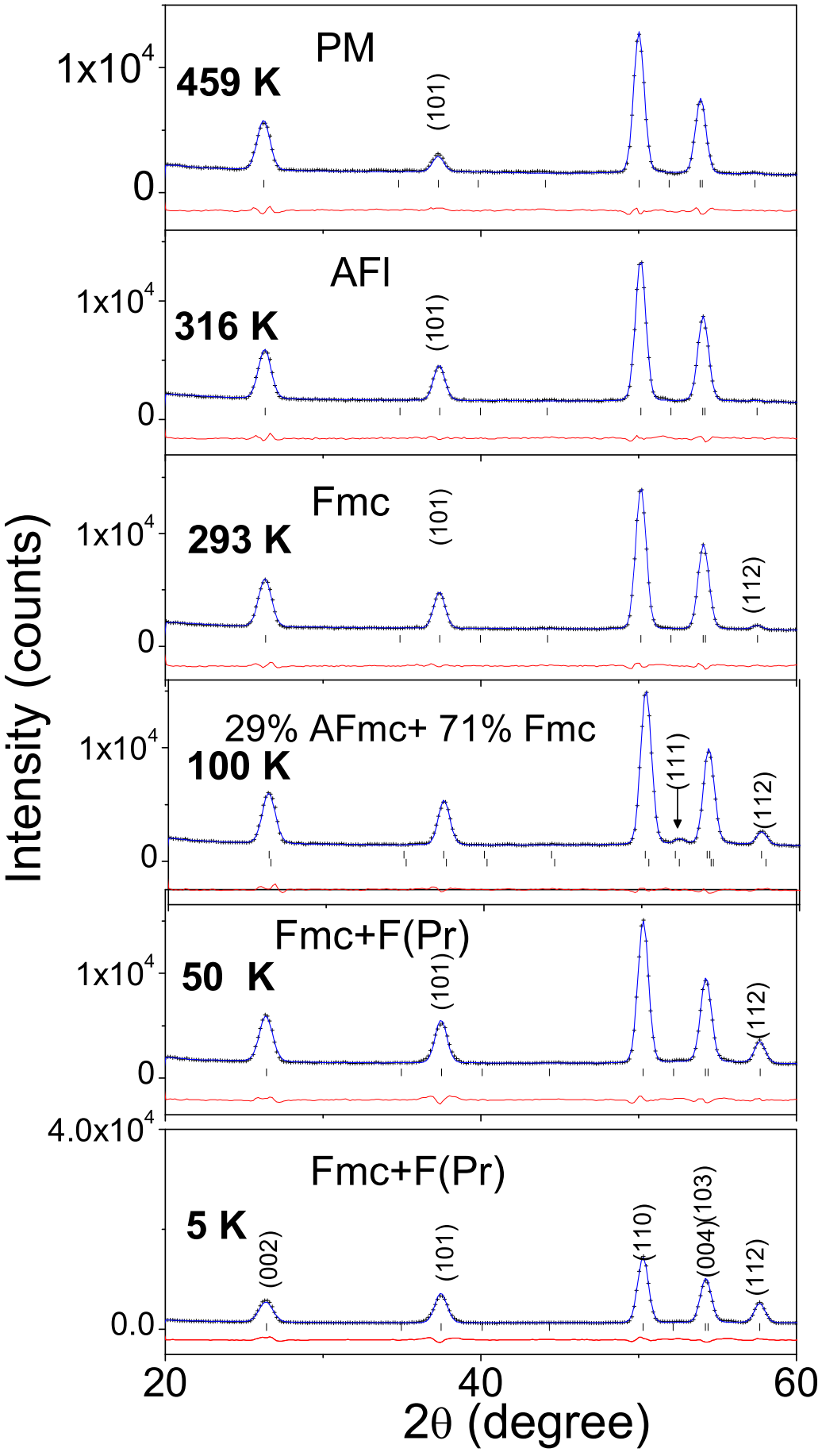

Figure 8 (figure8.eps)

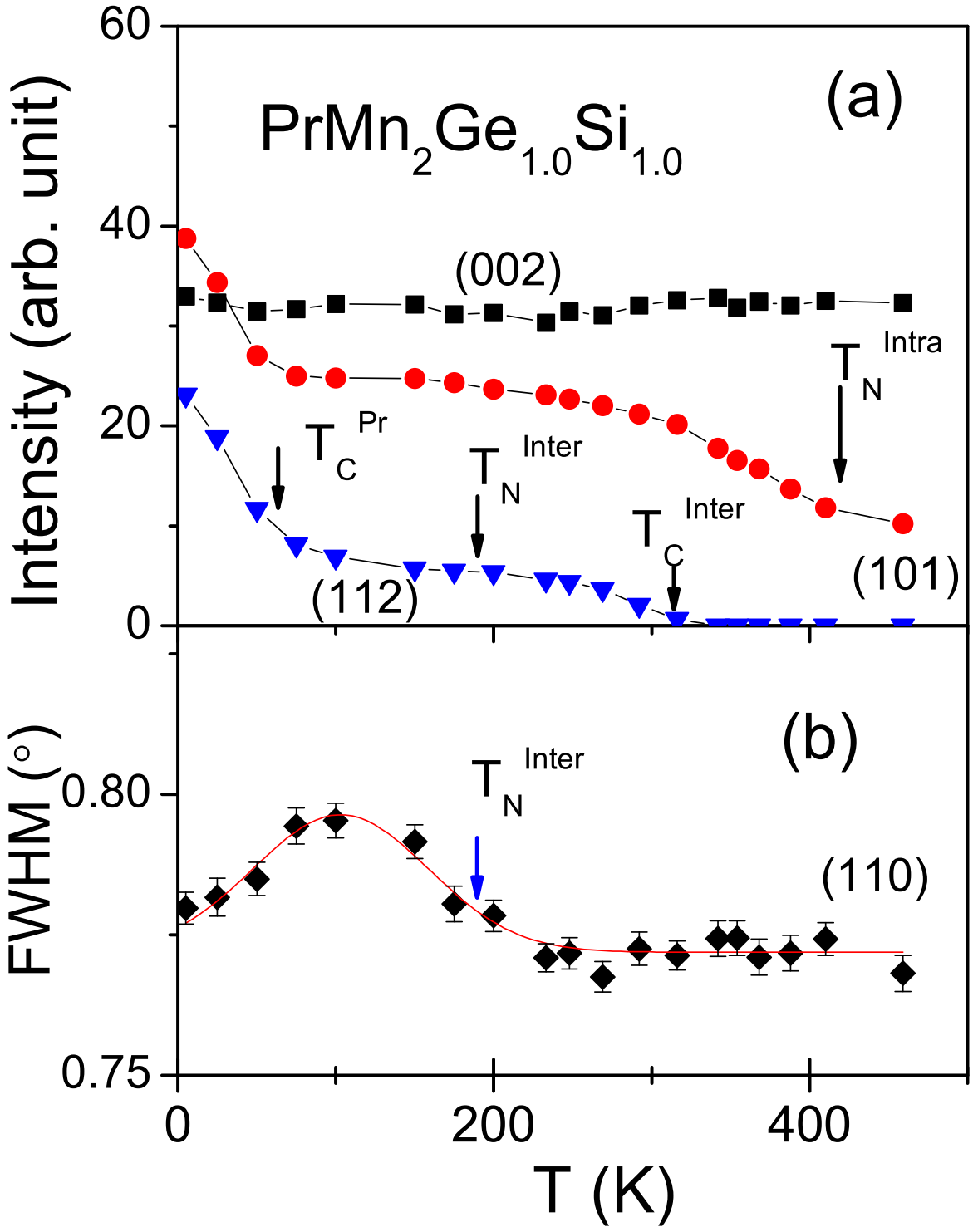

Figure 9 (figure9ab.eps)

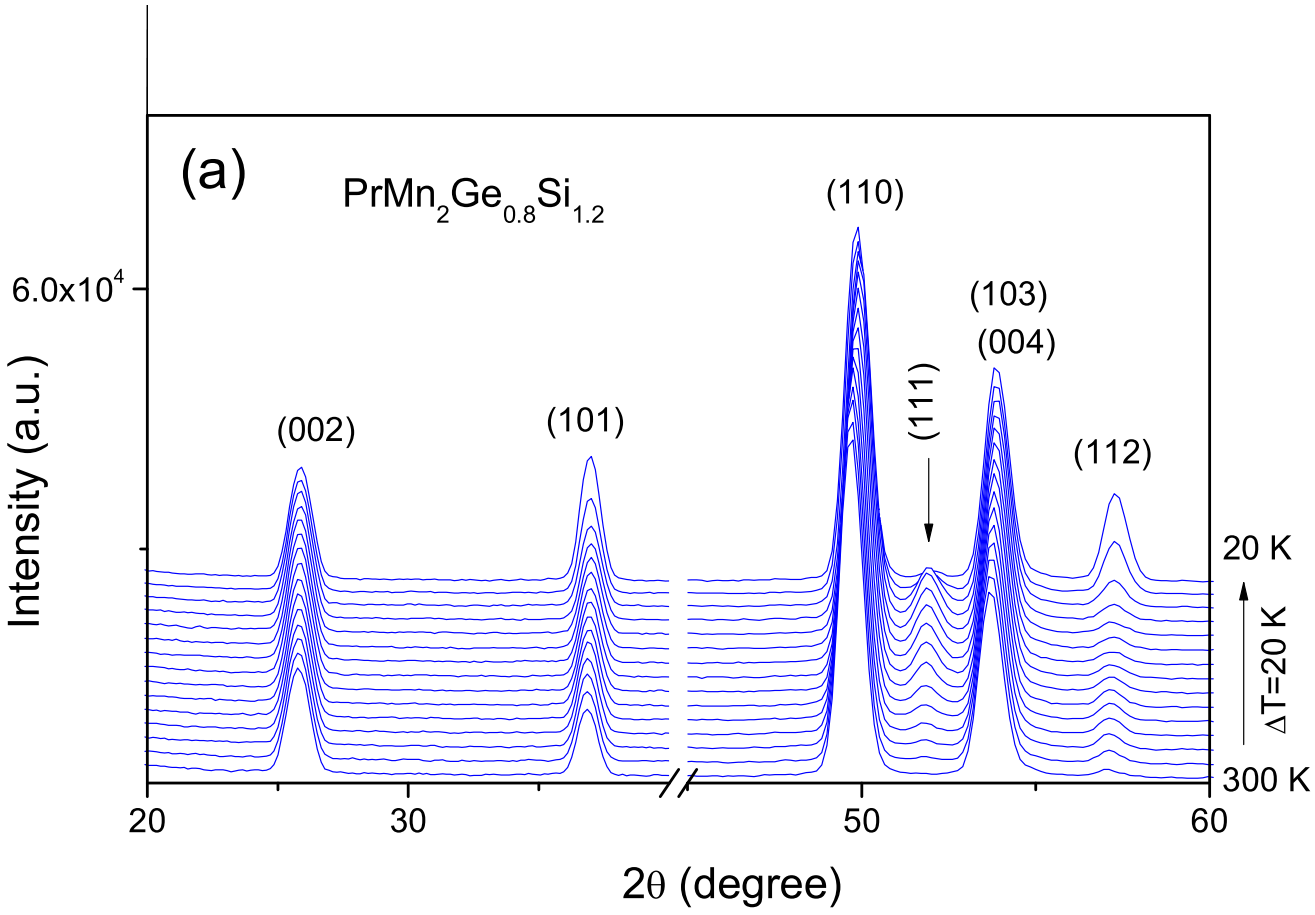

Figure 10a (figure10a.eps)

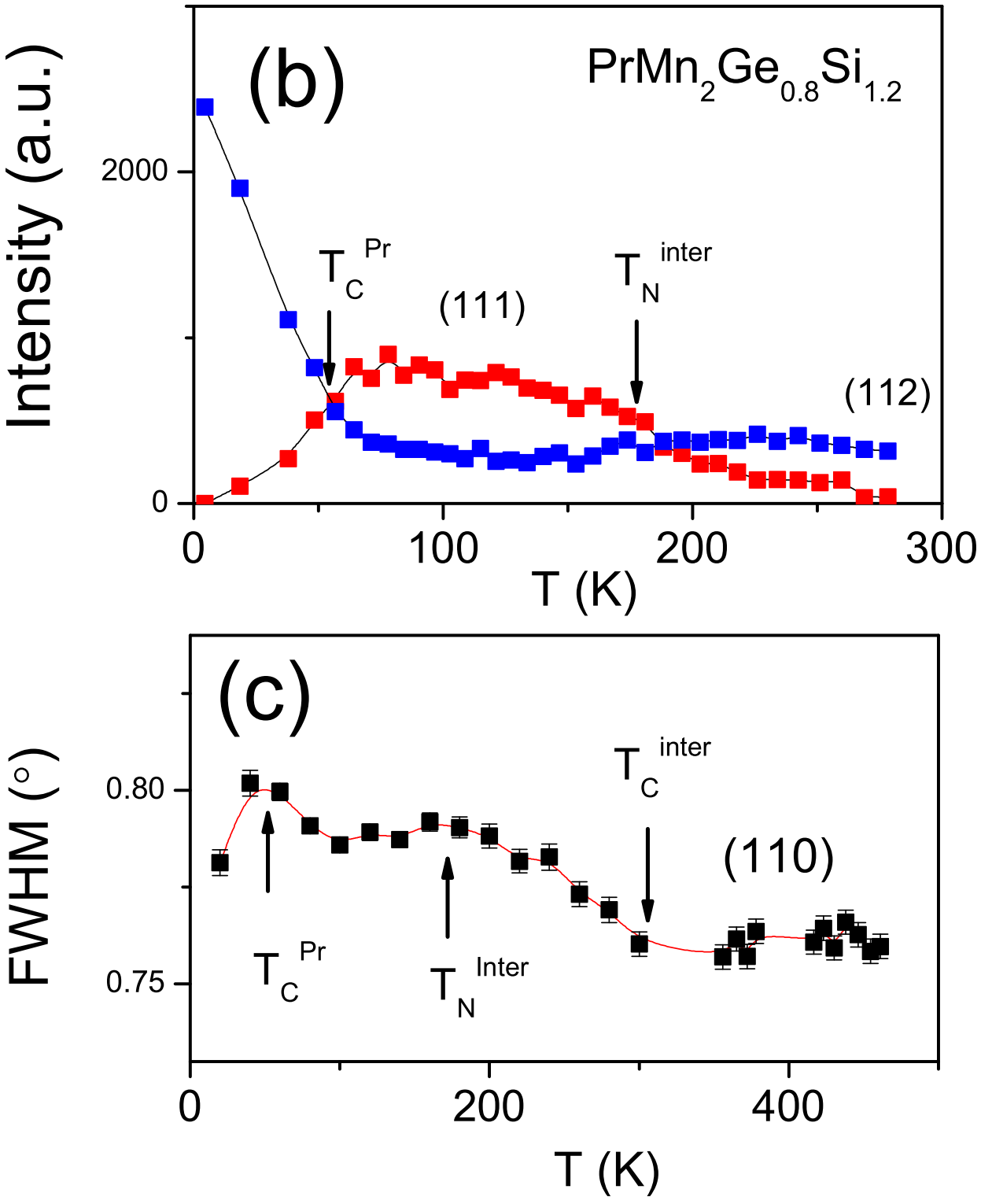

Figure 10bc (figure10bc.eps)

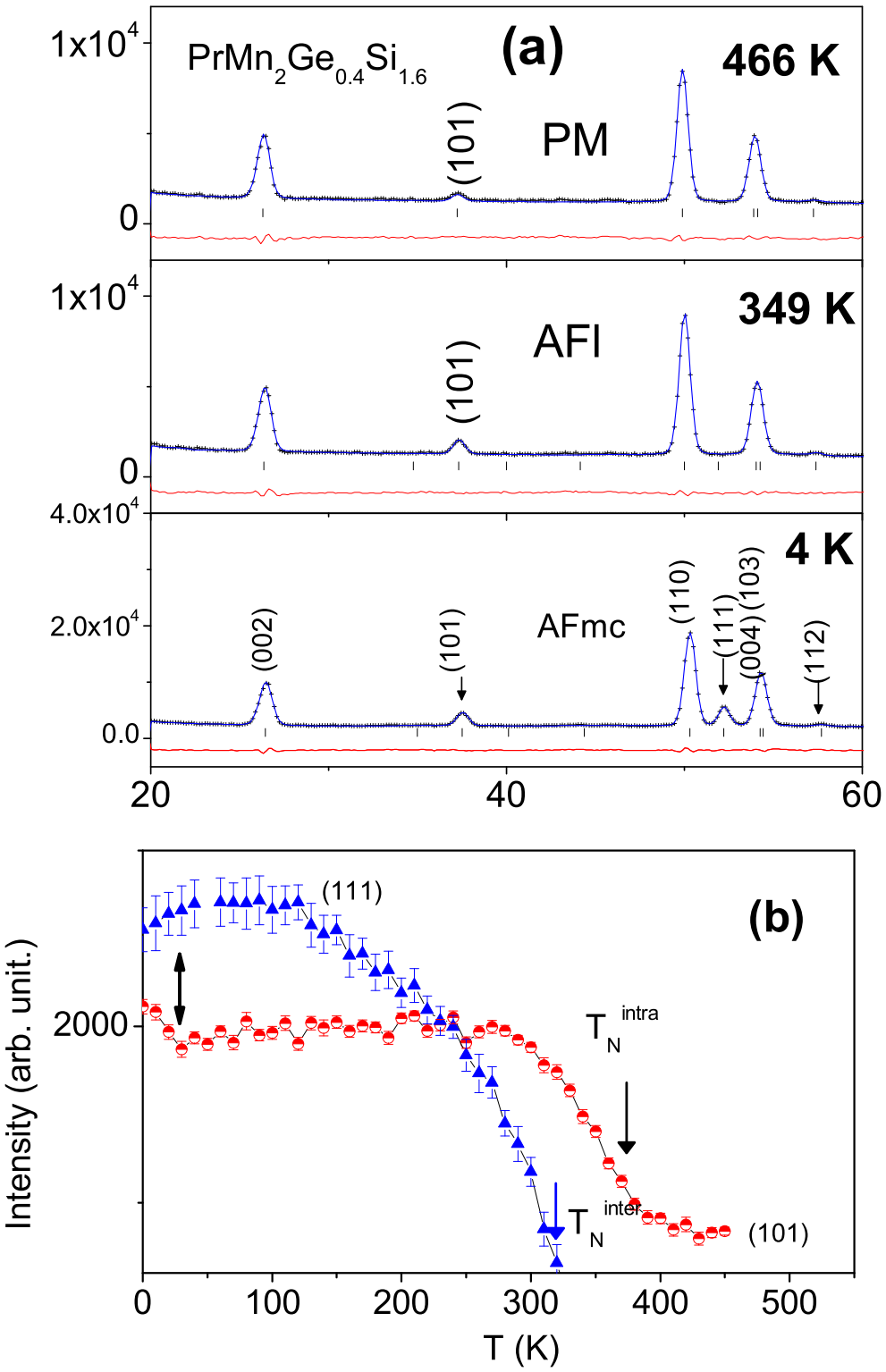

Figure 11 (figure11ab.eps)

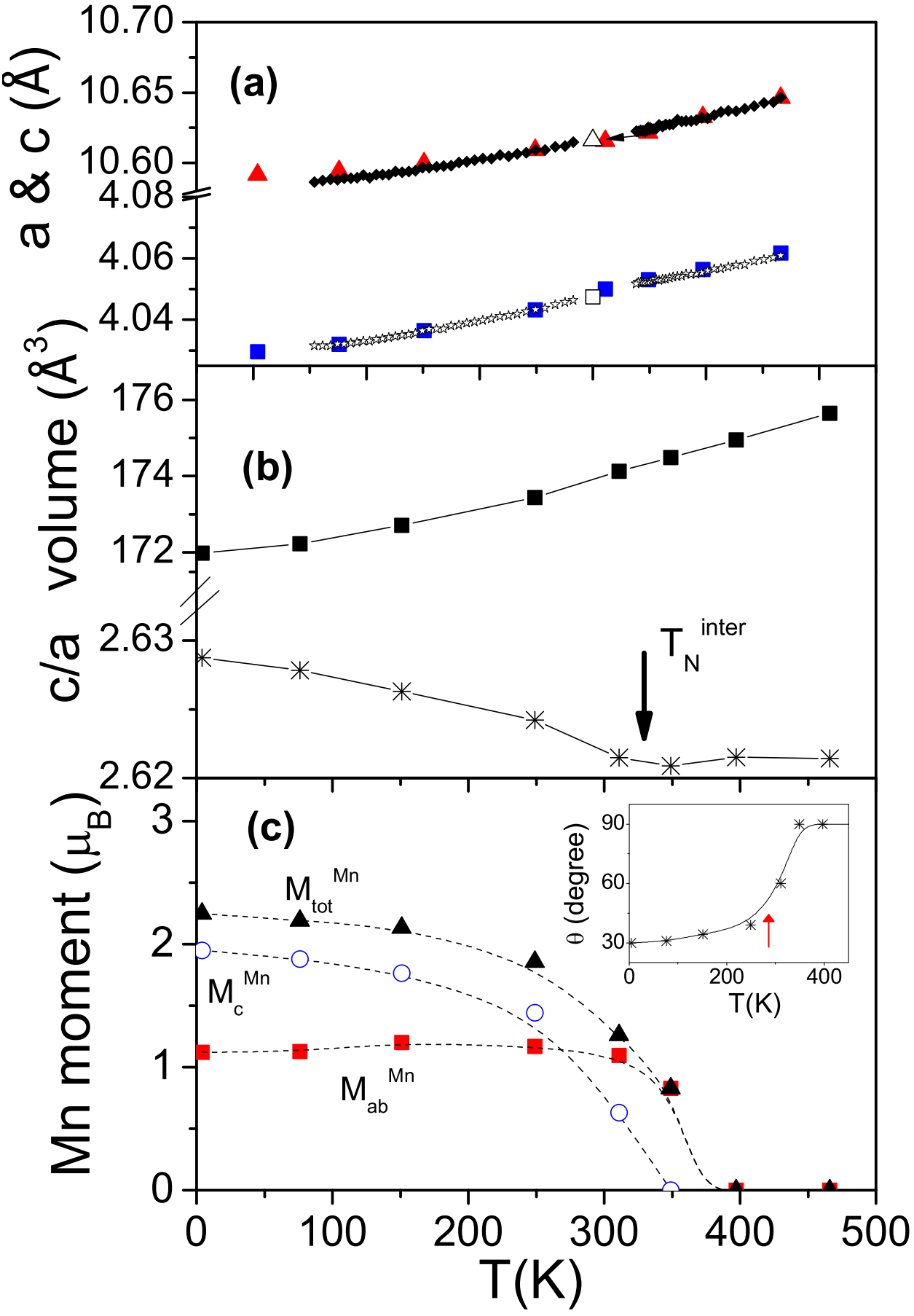

Figure 12 (figure12abc.eps)

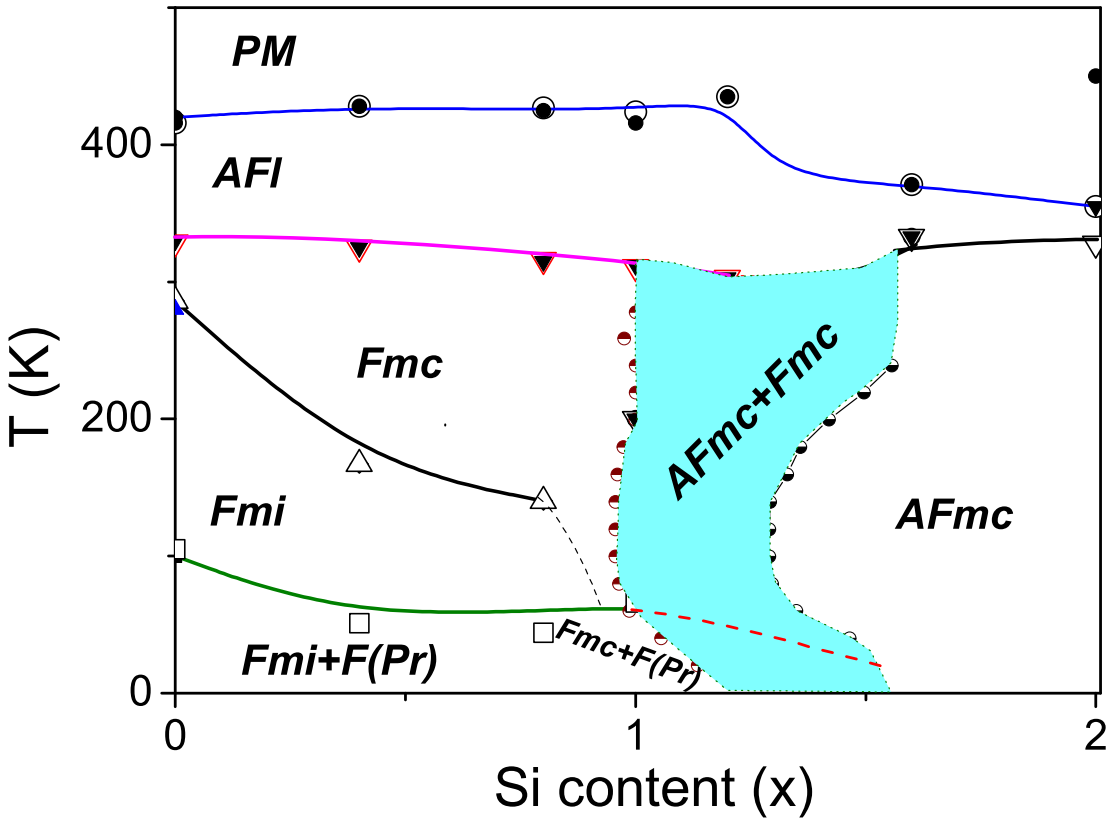

Figure 13 (figure13.eps)